nature neuroscience

ARTICLES

https://doi.org/10.1038/s41593-020-0614-x

Hippocampal neurons represent events as transferable units of experience

Chen Sun[1]✉, Wannan Yang[2], Jared Martin[1] and Susumu Tonegawa[1,3]✉

The brain codes continuous spatial, temporal and sensory changes in daily experience. Recent studies suggest that the brain also tracks experience as segmented subdivisions (events), but the neural basis for encoding events remains unclear. Here, we designed a maze for mice, composed of four materially indistinguishable lap events, and identify hippocampal CA1 neurons whose activity are modulated not only by spatial location but also lap number. These 'event-specific rate remapping' (ESR) cells remain lap-specific even when the maze length is unpredictably altered within trials, which suggests that ESR cells treat lap events as fundamental units. The activity pattern of ESR cells is reused to represent lap events when the maze geometry is altered from square to circle, which suggests that it helps transfer knowledge between experiences. ESR activity is separately manipulable from spatial activity, and may therefore constitute an independent hippocampal code: an 'event code' dedicated to organizing experience by events as discrete and transferable units.

How is daily experience represented in the brain? Most daily experiences involve traveling to different places and/or seeing different things, and so contain a multitude of spatial and sensory variations (Fig. 1a, top and middle). Hippocampal cells monitor these continuous changes in space, passing time and sensory stimuli[1–5].

Meanwhile others, based on recent human imaging studies[6–9], have suggested that besides tracking the continuously changing sensory environment, the brain tracks daily experience as a chain of discrete, segmented subdivisions or events. Each event arises as a discrete epoch of experience, with its continuous sensory and spatial changes grouped together as a unit. It has been suggested that events are abstract and generalizable entities and can be divorced from specific sensory details[10–13]. Take dining in a restaurant as an example. Two different dinner experiences can share the same set of events; that is, eating an appetizer, main course and dessert, even if they occur at different restaurants, involve different foods and last varying amounts of time (Fig. 1a, middle). In other words, each of these events has a degree of invariance to the variations of their actual physical and sensory contents. Instead, these events are defined by the abstract, ordered relationships to one another; that is, an appetizer is eaten first, followed by a main dish, which is followed by dessert. This allows events to describe widely varying experiences in a generalized manner. Encoding these abstract events is important to behave perspicaciously in the world.

Beyond representing continuous changes in space, there is evidence to indicate that hippocampal neurons encode broader episodic information, including changes in sensory cues[14] and past and future trajectories[15,16]. Hippocampal neurons encode this broader episodic information by changing the activity rate at a given place field (rate remapping). However, neural representations dedicated to encoding events as units of experience, separate from the tracking of the immediate continuous environment, remain poorly understood.

In this study, we found a hippocampal representation that treats events as discrete units of experience and show that these event representations can be transferred between different experiences. We also show that this representation is reciprocally and independently manipulable from continuous representation of space.

Results

Task design to study the segmentation of experience into units. With oft-used behavioral paradigms that involve changes in spatial[14–17] and sensory variables[18,19], it is difficult to separately identify neurons that track discrete and unitary events from those that track continuous sensory stimuli or spatial differences. For these reasons, we designed a repetitive behavioral task in which sensory cues and spatial trajectories were kept constant for multiple events (Fig. 1a,d). This allowed the influence of events as fundamental units to be separated from the influence of changing sensory or spatial information.

In our task, mice repeatedly ran through a square maze subdivided into four laps per trial (Fig. 1d). A reward was delivered at the onset of lap 1 of every trial, as a single temporal cue, with the subsequent three laps unrewarded. Salient stimuli can potentially serve as boundaries between events[9,17]; therefore, it is possible that reward box visits may serve as event boundaries between lap events. In fact, these mice visited the reward box after every lap, regardless of whether a reward was delivered (Extended Data Fig. 1a, left). We tested whether there were specific neurons that track lap events as discrete units of experience.

An adeno-associated virus (AAV) expressing the calcium indicator GCaMP6f (AAV2/5-Syn-flex-GCaMP6f-WPRE-SV40)[20] was injected into the dorsal CA1 (dCA1) of the hippocampus in *Wfs1* (Wolframin-1) promoter-driven Cre transgenic mice[21,22]. A microendoscope was implanted above the dCA1 (ref. [23]) to enable long-term calcium imaging in freely moving mice (Fig. 1b,c). We recorded calcium activity and characterized the spatial selectivity of CA1 neurons (Extended Data Fig. 1c) as mice navigated the square maze (Fig. 1d). During testing, animals completed 15–20 trials (60–80 laps) in succession. On average, test mice took 98 s to complete one trial (Extended Data Fig. 1a, right). For each neuron

[1]RIKEN-MIT Laboratory for Neural Circuit Genetics at the Picower Institute for Learning and Memory, Department of Biology and Department of Brain and Cognitive Sciences, Massachusetts Institute of Technology, Cambridge, MA, USA. [2]Center for Neural Science, New York University, New York, NY, USA. [3]Howard Hughes Medical Institute at Massachusetts Institute of Technology, Cambridge, MA, USA. ✉e-mail: sunchipsster@gmail.com; tonegawa@mit.edu

during each of the four laps, we calculated its average calcium activity level during moving periods (>4 cm s^{-1}) within spatial bins that tiled the maze (Methods). In total, 72% (2,509 out of 3,506) of CA1 cells from 14 animals were significant place cells. Some neurons were most active during reward consumption (lap 1) in the reward box (see Extended Data Fig. 1d for examples of reward-driven neurons); these cells were excluded from further analysis because they were active in direct response to the reward (Methods). In general, neurons that were active in the start box during non-rewarded laps, or in the maze, were active at the same location on every lap, but showed higher activity for a specific lap compared with other laps (Fig. 1e; Extended Data Fig. 1b). Here, we show the trial-by-trial calcium activities of example neurons for each of the four laps. Indeed, example neurons showed robustly higher activity during a particular lap across trials (Fig. 1f; Extended Data Fig. 1e).

Since CA1 activity is sensitive to a variety of behavioral variables, including spatial location[2], running speed[24,25] and head direction[25,26] (Extended Data Fig. 2b,c), we fitted the activity of each neuron to a linear model incorporating the spatial location, head direction and running speed of the animal (Methods) to investigate whether these modeled variables were enough to account for the lap preference. We then calculated the remaining calcium activity across four laps that was not accounted for by the model; we refer to this activity as model-corrected (MC) calcium activity (Fig. 1g). Each CA1 cell had a lap number during which the cell had the highest activity rate (its preferred lap), and in 30% of CA1 cells (1,055 out of 3,506 cells, $n=14$ mice; see Supplementary Fig. 1 for results for individual mice), this peak, lap-specific MC activity was significantly different (outside the 95th confidence interval) compared to shuffles. Although CA1 calcium activity exhibited stochasticity in its trial-by-trial activation (Fig. 1f; Extended Data Fig. 1e), these significant lap-modulated CA1 cells exhibited a systematic lap-modulated pattern that was robust across trials (Extended Data Fig. 3b). As a control comparison, the percentage of lap-modulated CA1 cells was reduced when reward was given every lap (9% (101 out of 1,072 cells), $n=5$ animals; Fig. 1i–k). Within the confines of the four identical lap task structure, this lap-event-specific MC activity manifested as a sequence of rate remapping[14–16] over a constant place-field location. These cells are henceforth called ESR cells. All the other CA1 cells were considered non-ESR cells. To study the lap-modulated calcium activity pattern for a given ESR cell, we compiled its lap-modulated MC activity in the peak spatial bin (Methods) for all four laps; this sequence of differential activity levels across the four laps is referred to as the ESR activity pattern (Fig. 1g, bottom). For the rest of this study, we investigated the features of the experience that give rise to the ESR phenomenon.

For a set of five animals that were exposed to the four-lap-per-trial task for the first time, the percentage of ESR cells was 17% (176 out of 1,008 cells, $n=5$ mice), but following 8 days of training on the lap task, the proportion rose to 29% for these same mice (335 out of 1,168 cells; Extended Data Fig. 4c–d; $\chi^2=37.9$, $P=7.4\times10^{-10}$), which shows that ESR activity patterns are learned. Correspondingly, mice did not run at increased speed during the fourth lap compared with the first lap during the first exposure to the four-lap task, but they ran significantly faster during the fourth lap compared with the first lap following 8 days of training on the four-lap task (Extended Data Fig. 4e). In addition, once mice had been well trained, if reward was unexpectedly delayed by an extra lap on some trials, mice still ran significantly faster on the fourth lap compared with the first lap, but also ran significantly slower during this extra fifth lap compared with the fourth lap, which suggests that animals anticipated reward exactly at the end of the fourth lap (Extended Data Fig. 4b).

We tracked ESR cells across days (Extended Data Fig. 5) to examine the preservation of ESR activity patterns. For every individual ESR cell on day 1, we defined an index for how much the ESR activity patterns are preserved across days as the Pearson's correlation of its ESR activity pattern on day 1 versus day 2. The proportion of ESR cells that were highly preserved across days was significantly greater than chance for each of the separate populations of lap 1 cells, lap 2 cells, lap 3 cells and lap 4 cells (Fig. 2e; see Fig. 2a–c for example cells; see Extended Data Fig. 6a for the analogous raw change in fluorescence ($\Delta F/F$) results without model correction; Methods). The ESR activity patterns for laps 1–4 were highly preserved even when half the trials were eliminated (Extended Data Fig. 7a–c), as measured by the ESR correlation index. Generally, lap 1 cells were more highly represented (Fig. 1h) compared with laps 2, 3 and 4 cells, although all four subpopulations of lap-specific cells were significantly preserved in their own right (Fig. 2e; Extended Data Fig. 6a).

ESR treats events as fundamental units of the experience. Several key results support the notion that ESR tracks lap events as discrete units of the experience, separate from the continuous moments that also make up the experience. Since previous studies[2–5] have shown that the hippocampus encodes continuously changing variables, we investigated in detail the relationship between ESR activity and several continuous episodic variables. Instead of tracking lap events,

Fig. 1 | Experimental design to study the segmentation of experience into units. a, Illustration of experience as a sequence of continuous, moment-to-moment variations in space, time and sensory stimuli (top) or as a sequence of discrete events as fundamental units of the experience (middle). In our behavioral task (bottom), a skeletal experience stripped of sensory and spatial differences was used to identify neuronal representations that track events as fundamental units. **b**, Schematic of implantation of the microendoscope into the dCA1 of *Wfs1*-Cre mice with AAV2/5-Syn-flex-GCaMP6f-WPRE-SV40 virus injected in the dCA1 for imaging CA1 pyramidal cells. **c**, Top: a coronal section of hippocampus showing the area of cortex aspiration (white dotted line) and labeled Wfs1$^+$ cells (green). The image is representative of aspiration surgeries from $n=14$ mice. Bottom: $\Delta F/F$ calcium traces of $n=15$ Wfs1$^+$ (pyramidal) cells in the CA1, where red traces denote significant calcium transients. **d**, During the standard four-lap-per-trial experiment, reward was delivered to the animal at the beginning of lap 1 in the reward box once every four laps. **e**, CA1 calcium activity sorted by spatial position and lap number showed activity in the same place on every lap, but displayed a higher activity level during a specific lap compared with other laps (263 cells from an example animal shown). The red label on the *x* axis indicates the reward box spatial bin, and the green label on the *x* axis indicates the 100-cm-long maze track. **f**, Trial-by-trial calcium activity of lap-specific neurons for example laps 1, 2, 3 and 4 (L1–L4), organized by the location of activity along the track and by lap number. The top panels show trial-by-trial calcium activities, while the bottom panels show trial-averaged calcium activities (mean ± s.e.m.). The standard error was cut off at 0 because negative activity does not exist. **g**, Model correction of lap-dependent neuronal activity. Top left: example neuron with the raw calcium activity level (light blue) sorted by the lap number and spatial bin. Bottom left: the peak spatial bin was analyzed to detect lap-specific calcium activity. The plotted calcium rate was explained by the speed and head orientation fitted linear model (pink trace; see Methods). Top and bottom right: the same as the left charts, but plotted with the lap-specific remaining calcium rate after the linear model was subtracted, resulting in the MC calcium activity. **h**, Summary statistics of the percentage of ESR cells in the entire CA1 pyramidal population that were tuned to laps 1, 2, 3 or 4 in the standard 4-lap experiment ($n=14$ animals). **i**–**k**, For this set of experiments, reward was given to the animal at every lap (**i**). The percentage of significant ESR cells (9%; 101 out of 1,072 cells) was significantly reduced when reward was given at every lap (1R/L) compared with the same animals running the standard 4-lap-per-trial task (1R/4L; 28%; 371 out of 1,328 cells) ($\chi^2=128.7$, $^{***}P<1\times10^{-16}$, blue lines represent five mice) (**j**). Summary statistics of the percentage of ESR cells in the entire CA1 pyramidal population that were tuned to laps 1, 2, 3 or 4 during the reward every lap experiment (**k**).

could ESR cells be tracking a particular duration of time since the start of the trial? Time cells[3,4] require a reliable temporal delay period, otherwise they do not arise[4]. Because the animals in our task were allowed to behave freely, and took unpredictable and variable durations to complete the trials of the task (Extended Data Fig. 8a,b) and ran at varying speeds (Extended Data Fig. 9a,b, purple), ESR cells were unlikely to act as time cells in our task. Could ESR cells instead be representing the total distance continually traveled along the course of the four-lap task since the start of the trial? When we elongated the maze in one dimension to twice the usual length

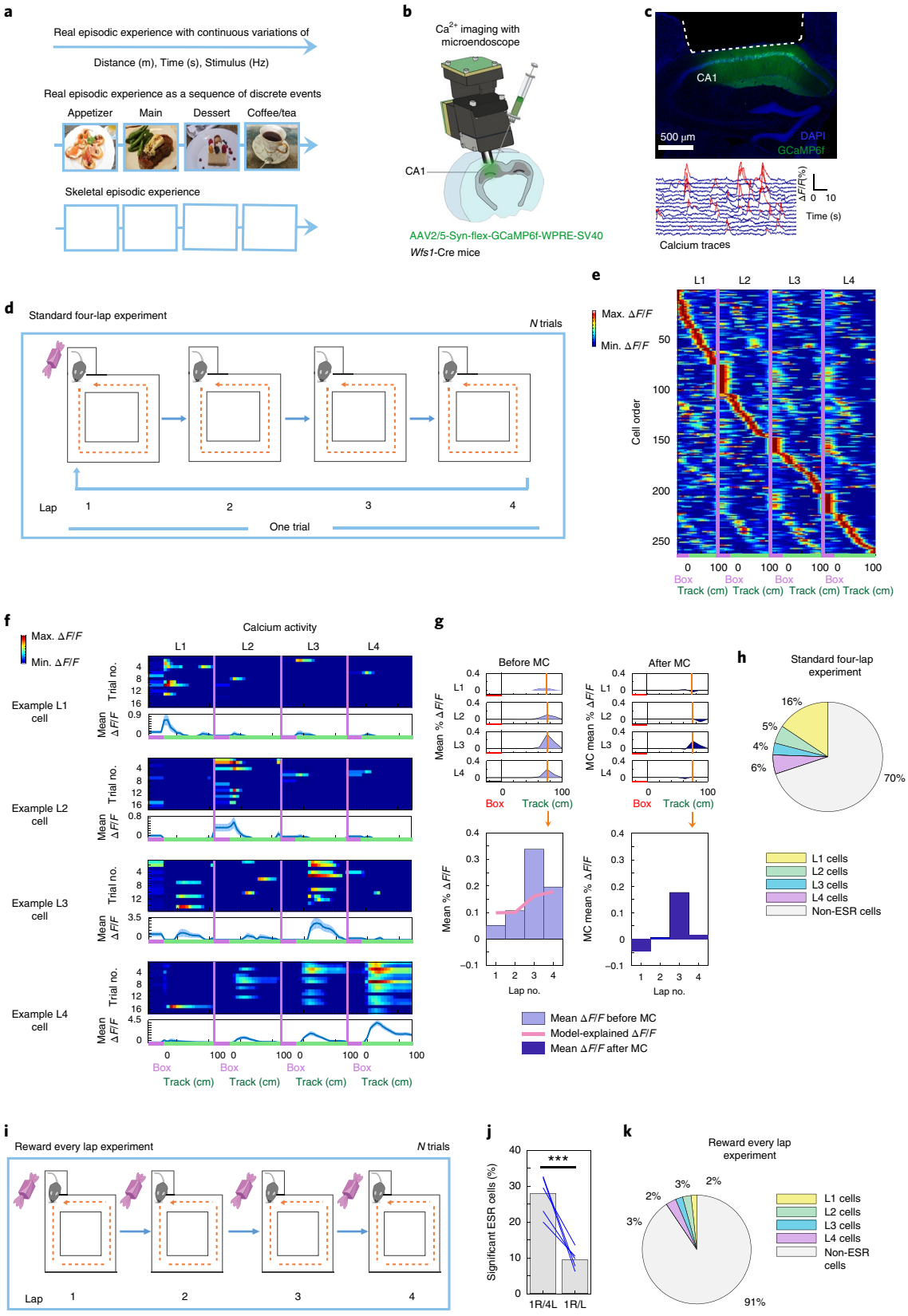

(Extended Data Fig. 8c; Methods, "Task-specific training"), the ESR activity patterns were still significantly preserved across days (Extended Data Fig. 8f; see Extended Data Fig. 8d,e for example cells; see Extended Data Fig. 6b for raw $\Delta F/F$ results), which suggests that it is unlikely that ESR cells directly track the continuous distance traveled.

We conducted another experiment to investigate whether laps are treated as units of experience. A four-lap-per-trial task was conducted in which the maze was elongated on pseudorandomly chosen laps of pseudorandomly chosen trials (see Fig. 3a, left, for trial types; see Fig. 3b for the full task schedule; Methods). Importantly, this maze was largely stripped of predictability in traveled distance, but the four discrete-lap structure was preserved. A total of 27% of CA1 cells (306 out of 1,128 cells, $n=6$ animals) active in all trial types of this experiment were significant ESR cells. For these cells, their ESR activity pattern during the standard (short SSSS sequence, where S denotes a short lap) trials was preserved during each of the pseudorandomly elongated trial types (Fig. 3c–f; see Fig. 3a, right, for an example cell; see Extended Data Fig. 6c for raw $\Delta F/F$ results). Thus, ESR activity of this sizeable population of CA1 cells was unperturbed by arbitrary and unpredicted variations within the relevant lap event or even variations within neighboring (preceding and succeeding) lap events (illustrated in Fig. 3a, middle). For these cells, their ESR activity was preserved even during SSLL sequence (where L denotes a long lap) trials compared with LLSS trials (Fig. 3f), which were trials that had the same total distance (Fig. 3a, middle) but had different internal segmentation into long and short laps. Therefore, ESR activity treats these lap events as separate units of the experience that are unaffected by spatiotemporal variations within the current or neighboring event units.

ESR activity is transferrable between experiences. The results thus far suggest that the lap events tracked by ESR have a generalizable nature and are robust against continuous variabilities like time (Extended Data Fig. 8a,b) or distance (Fig. 3a–f; Extended Data Fig. 8c–f). If this notion is correct, then we predict that ESR activity should exhibit a degree of independence from sensory and spatial content. To test this concept, we conducted a 2-day experiment with the four-lap-per-reward task on two geometrically distinct mazes. The standard square maze was used on the first day and a circular maze was used on the second day (Fig. 4a; Methods, "Task-specific training"). The spatial activity of ESR cells globally remapped on the circular maze compared with the standard square maze as a result of the different geometry of the maze (Figs. 4e,g (blue histogram); see Fig. 4c for example cells; see Extended Data Fig. 6d for raw $\Delta F/F$ results). Nevertheless, a significant proportion of ESR cells tracked circular laps using the same lap-specific activity pattern as the corresponding square maze laps (38% (176 out of 461 total cells), with ESR correlation >0.6 across days; Fig. 4f; see Fig. 4b,d for example cells). Thus, the knowledge of lap specificity acquired during the square maze was reused (transferred) when the animals were faced with the circular maze.

To further test the generalizable nature of these lap events, we modified the repetitive square maze by adding spatial trajectory variation. A 2-day experiment was conducted in which the four-lap-per-reward was preserved on the second day, whereas the spatial trajectories were altered every two laps (Extended Data Fig. 10a; Methods, "Task-specific training"). Here, a significant proportion of lap 1–4 ESR cells still had preserved ESR activity across sessions (Extended Data Fig. 10d; see Extended Data Fig. 6e for raw $\Delta F/F$ results), and coded laps 1–4 despite the animals experiencing differential spatial trajectories on different laps.

ESR tracks the relationships between events. ESR does not reflect precise sensory information per se, so we hypothesized that it might instead reflect more generalized information from the structure of the task, such as the ordered relationships[27,28] between the event units. This was suggested by the fact that the four lap events of our task are identical to one another in their sensory and spatial content, yet, ESR activity still reliably distinguished each of the four lap numbers (laps 1, 2, 3 and 4). To further test the hypothesis that ESR tracks the ordered relationships between events, we conducted two experiments.

First, we conducted an experiment in which the relationships between lap events were abolished. The standard four-lap-per-trial experiment was conducted on the first day, but the once-in-four lap delivery of the reward (which serves as a temporal marker) was perturbed on the second day and instead the reward was provided every lap (Fig. 5a). We found that preservation of the ESR activity pattern across laps 1, 2, 3 and 4 was significantly abolished across days (Fig. 5b,c).

Second, we conducted an experiment in which the relationships between the lap events were more subtly perturbed, and asked how this affects ESR activity. The standard four-lap-per-trial experiment was conducted on the first day and a non-rewarded fifth lap was added to all the trials on the second day before reward presentation (Fig. 5d, Methods, "Task-specific training"). On day 2, lap 1 and 2 cells had preserved ESR activity despite the added lap (Fig. 5e; see Extended Data Fig. 6f for raw $\Delta F/F$ results). By contrast, lap 3 cells were abruptly and discretely perturbed (Fig. 5e,f). Indeed, a significant proportion of lap 3 cells shifted to track lap 4 (Fig. 5g,h; 31% (17 out of 55 cells), $n=4$ mice). By contrast, only 9% (5 out of 55) of cells maintained their lap 3 preference.

Similarly, lap 4 cells shifted to track lap 5 (Fig. 5i,j). Although, overall, the pattern of most lap 4 cell activity across the 2 days was well correlated (Fig. 5e), a significant proportion of lap 4 cells (70% (42 out of 60 cells), $n=4$ mice, $P<1\times10^{-4}$ compared to shuffling) showed a significant decrease in overall activity level during lap 4 on day 2 (Fig. 5k; see Extended Data Fig. 6f, right, for raw $\Delta F/F$ results), but also showed an apparent concomitant restoration of activity level during lap 5 (Fig. 5l; see Extended Data Fig. 6f, right, for raw $\Delta F/F$ results). This decrease in activity during lap 4, and shift in activity by precisely one lap unit, reflects the fact that the

Fig. 2 | Lap 1, 2, 3 and 4 ESR cells are reliably preserved across days. a–c, Trial-by-trial calcium activities of lap-specific neurons for example laps 1, 2, 3 and 4, matched across two consecutive days (**a**). The top panels show trial-by-trial calcium activities, while the bottom panels show trial-averaged calcium activities (mean ± s.e.m.). The number of trials for each cell is indicated in each panel. The standard error was cut off at 0 because negative activity does not exist. The spatial activity (**b**) and ESR activity (**c**), as measured by MC calcium activity, were calculated for these example neurons. For each example neuron, the Pearson's correlation between its ESR activity pattern across days 1 and 2 was computed (**c**, values in orange text). This ESR correlation serves as an index of how well the ESR pattern was preserved across days. **d**, The calcium activity of individual ESR cells sorted by spatial location on the track during day 1, with this cell order matched across days, affirm that preserved place fields occur across days (622 cells in total, $n=8$ animals). **e**, Summary data of Pearson's correlation of ESR activity across days for these individual cells, plotted separately for lap 1, 2, 3 and 4 cell populations. The ESR activity of each individual cell on day 1 correlated with its own ESR activity on day 2 is in orange. The ESR activity of each cell on day 1 correlated with the ESR activity of arbitrary cells (that is, shuffled cell identities) from day 2 is in gray. The proportion of cells with highly preserved ESR patterns across days (that is, cells with Pearson's $r>0.6$, outlined in blue boxes) was significantly greater compared to shuffles. χ^2 and P values are shown in the figure ($n=622$ cells in total). **f**, Individual cells show both high ESR correlations and high spatial correlations across days ($n=622$ cells).

fourth lap is no longer rewarded and that an extra lap is needed to fulfill the total requirement of 5 laps to receive a reward. By contrast, only 3% (2 out of 60) of cells maintained their lap 4 preference. Therefore, ESR tracks the skeletal structure of experience, whereby it tracks events as fundamental units and the ordered relationships between them.

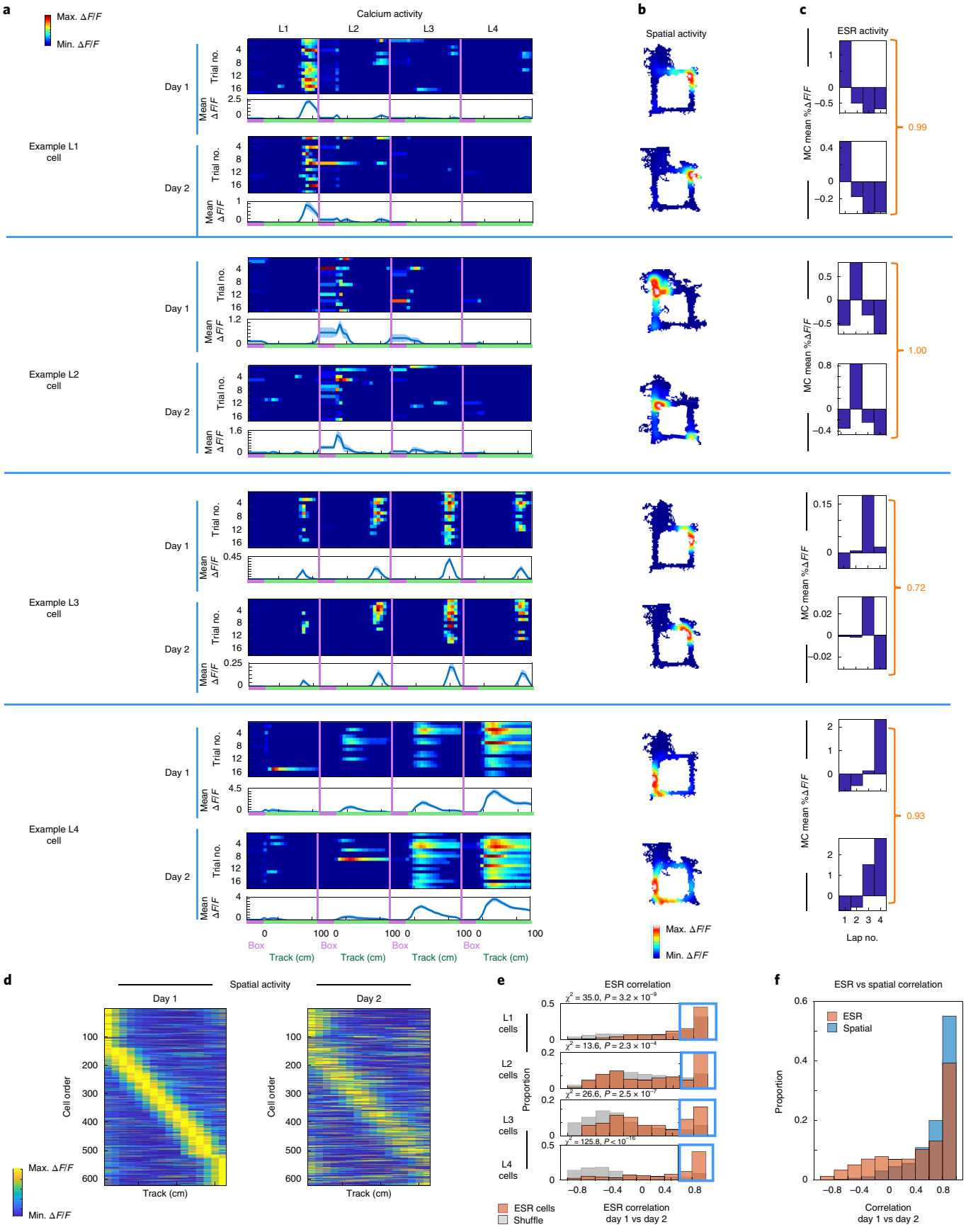

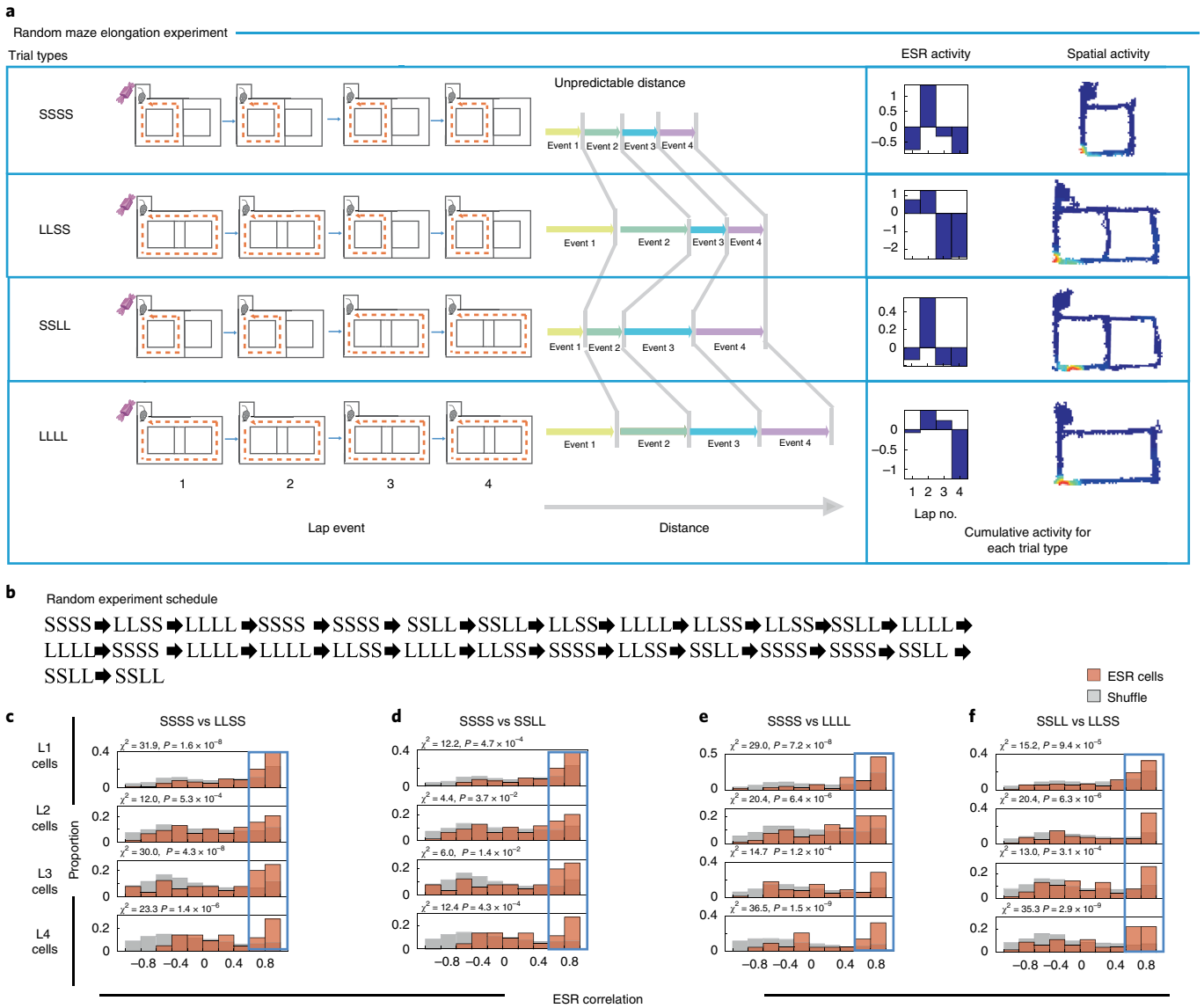

Fig. 3 | ESR treats events as fundamental units of experience. a, Left: four types of trials during the random maze elongation experiment: SSSS, LLSS, SSLL and LLLL. Each trial type has consistent four-laps-per-reward structure despite variability within the lap events. Right: an example L2 cell showing its ESR activity and spatial activity during each of these different experiments. **b**, Schematic of the pseudorandom experiment schedule, whereby a total of 28 trials were performed, with 7 trials pseudorandomly represented for each of the four types. **c**–**f**, ESR correlations of individual cells during standard four-lap trials (SSSS) versus LLSS trials (**c**), SSSS versus SSLL trials (**d**), SSSS versus LLLL trials (**e**) or SSLL versus LLSS trials (**f**) (the same 306 cells were used, $n = 6$ mice, for each separate trial type comparison). The proportion of cells with highly preserved ESR patterns across trial types (Pearson's $r > 0.6$, outlined in the blue boxes) was significantly greater compared to shuffles.

ESR activity and spatial activity are jointly but separately represented in the same cells. ESR activity and spatial activity occur jointly in the same cells. But what is the relationship between these two representations? Within the confines of the standard four-lap task (Fig. 1), ESR activity manifests as the differential activity rate during each of the different laps (Fig. 1e) at the same spatial field location; therefore, it is a form of rate remapping[4,14,15] (Fig. 1e; Extended Data Fig. 1b). We then investigated whether this ESR activity pattern is necessarily tied to its particular place-field location by testing whether ESR activity could be reciprocally and separately manipulable from the spatial activity.

When the maze and task were not altered across days, both ESR activity patterns and spatial activity patterns remained unperturbed (Fig. 2f,d). By contrast, as we previously showed, the four-lap task conducted on a circular maze geometry distorted the spatial activity, but ESR activity remained largely intact (Fig. 4g,c), which shows that ESR activity is not tied to its particular place-field location. Can the converse result, an alteration of ESR activity pattern without a concomitant alteration of the spatial activity pattern, be observed? First, perturbing the relationships between events by adding a lap (Fig. 5d) altered some ESR activity patterns (Fig. 5g–l; Fig. 5f, orange histogram), but spatial activity was still preserved in the same cells (Fig. 5f, blue histogram). Second, we investigated medial entorhinal cortex (MEC) axonal terminal inhibition in the CA1 and asked how it affects the ESR activity versus the spatial activity patterns. MEC input into the hippocampus has been implicated in the sequential organization of experiences[29–31], although this is not the only brain region to be

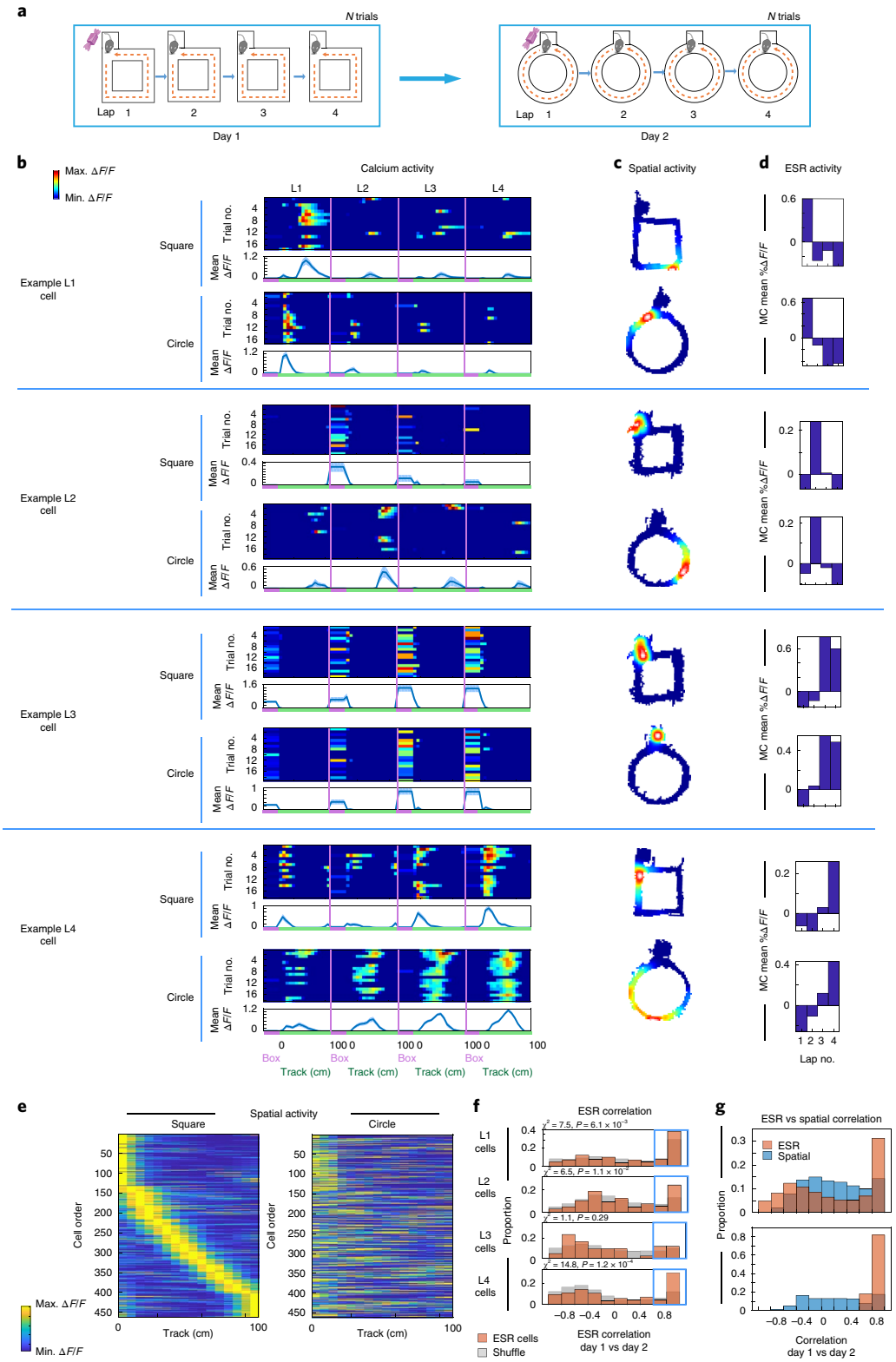

Fig. 4 | ESR tracks lap events despite changes in maze geometry. a, Schematic of the circular maze experiment. The standard square maze was used on day 1, and the circular maze was used on day 2. **b**–**d**, Example lap-specific neurons for example laps 1, 2, 3, and 4, with trial-by-trial calcium activities (**b**), spatial activities (**c**) and ESR activities (**d**) matched across the standard maze and the circular maze sessions. The number of trials for each cell is indicated in each panel in **b**. **e**, The calcium activity of individual ESR cells sorted by spatial location on the square linear track during day 1, with this cell order matched across days (461 cells, $n = 5$ mice). **f**, ESR correlations of these individual cells during the square maze versus circular maze sessions. The proportion of cells with highly preserved ESR patterns across days (Pearson's $r > 0.6$, outline in the blue boxes) was significantly greater compared to shuffles ($n = 461$ cells total). **g**, Top: individual cells showed high ESR correlations, while spatial fields remapped, during the circular maze experiment ($n = 461$ cells). Bottom: the same plot as above, but applied to the subpopulation of highly preserved (that is, ESR correlation > 0.6, see Fig. 2e for details) ESR cells; their spatial activity was also remapped ($n = 176$ cells).

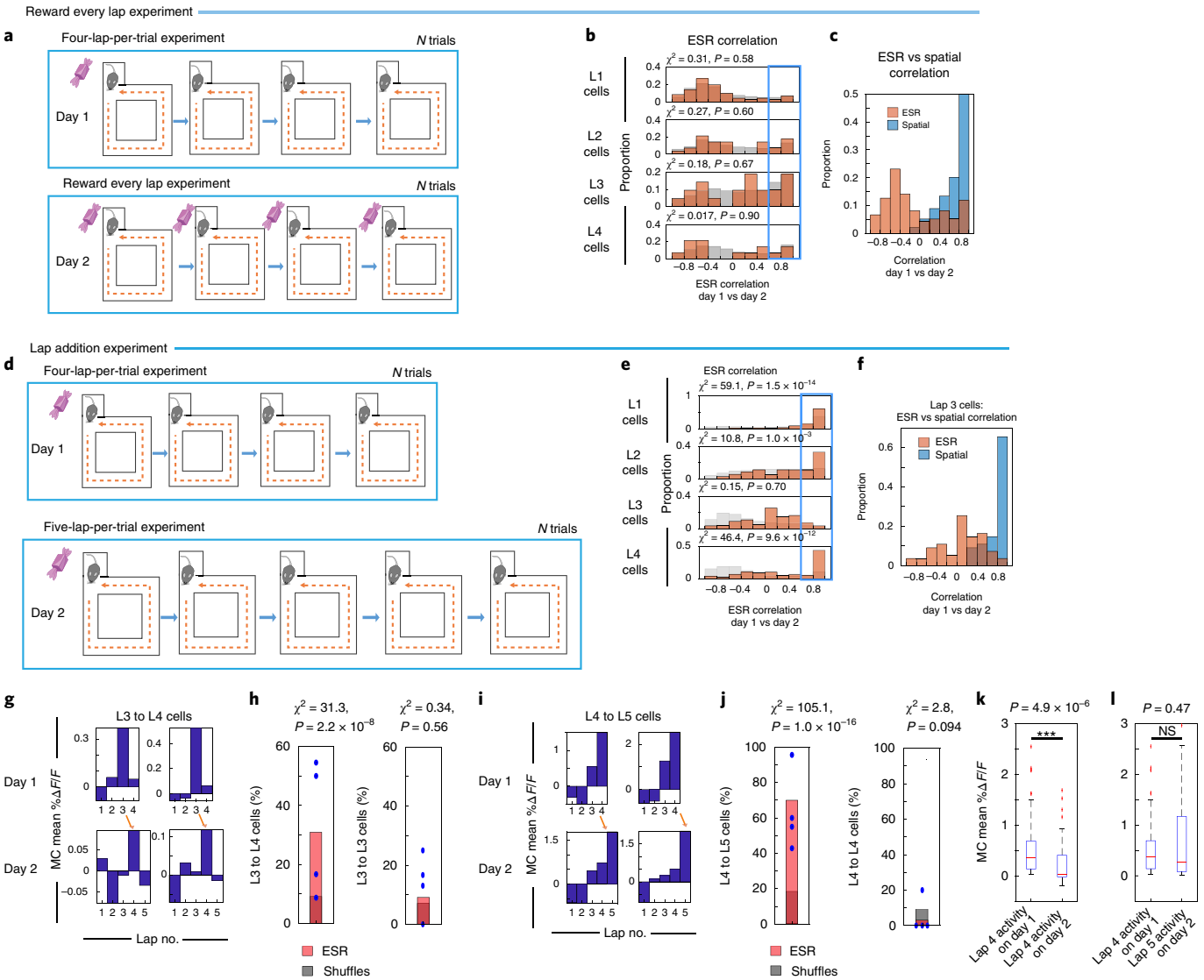

Fig. 5 | ESR tracks the relationships between events. a–c, This set of experiments used the reward every lap design. **a**, The standard four-lap-per-trial experiment was used on day 1; the reward every lap experiment was used on day 2. **b**, ESR correlations across the standard four-lap versus reward every lap experiment (134 cells, $n = 3$ mice). See Fig. 2e for a more detailed description and the methods. **c**, Individual cells showed high spatial correlation while ESR representations were perturbed during the four-lap versus reward every lap experiment ($n = 134$ cells). **d**, For the lap addition experiment, the standard four-lap-per-trial experiment was used on day 1, and the five-lap-per-trial experiment was used on day 2. **e**, ESR correlations across the four-lap and five-lap experiment sessions (382 cells, $n = 4$ mice). See Fig. 2e for description and methods. **f**, Individual L3 cells showed high spatial correlation while ESR representations were perturbed during the lap addition experiment (55 cells, $n = 4$ mice). **g**, Two example neurons matched across four-lap and five-lap experiment sessions that transformed from lap 3 to lap 4 preference. **h**, Percentage of cells that transformed from lap 3 to lap 4 preference (17 out of 55 cells, blue circles represent 4 mice). **i**, Two example neurons matched across four-lap and five-lap experiment sessions that transformed from lap 4 to lap 5 preference. **j**, Percentage of cells that transformed from lap 4 to lap 5 preference (42 out of 60 cells, blue circles represent 4 mice). **k**, The MC activity of cells from **j** during lap 4 on day 1 was significantly decreased during the same lap on day 2 (42 cells, Wilcoxon signed-rank test: $z = 4.57$). **l**, The MC activity of the cells from **j** during lap 4 on day 1 was not significantly different from the MC activity during lap 5 on day 2 (42 cells, Wilcoxon signed-rank test: $z = -0.72$). Box and whisker plots display the median, the 25th and 75th percentiles (box), and the maximum and minimum values (whiskers). ***$P < 0.001$; NS, not significant.

implicated[32,33]. Based on these earlier studies, a virus expressing inhibitory opsin (AAV2/2-EF1a-DIO-eNpHR3.0-mCherry) was bilaterally injected into the MEC subregion of *pOxr1*-Cre mice[34,35] (Fig. 6a,b). In addition, a virus expressing the calcium indicator GCaMP6f (AAV2/5-CamKII-GCaMP6f-WPRE-SV40) was unilaterally injected into the dCA1 of the same mice (Fig. 6a). An optoendoscope was implanted above the dCA1 to enable long-term calcium imaging and optogenetic inhibition of the axonal terminals from MEC neurons in the dCA1. The mice ran 28–40 trials of the four-lap task, whereby the trials alternated between optogenetic inactivation (light-on) and no inactivation (light-off) (Fig. 6c) of the MEC axonal terminals. Inactivation of MEC terminals in the dCA1 did not change the spatial activity patterns in the dCA1 (Fig. 6g,i (blue histogram); see Fig. 6e for example cells), which is consistent with previous studies[30]. However, this inactivation altered ESR activity patterns in the same cells (Fig. 6h,i (orange histogram); see Fig. 6d–f for example cells). By contrast, control mice that were injected with AAV2/2-EF1a-DIO-mCherry (that is, no eNpHR3.0 to inhibit opsin) had preserved ESR activity patterns across light-on and light off trials (Fig. 6j,k).

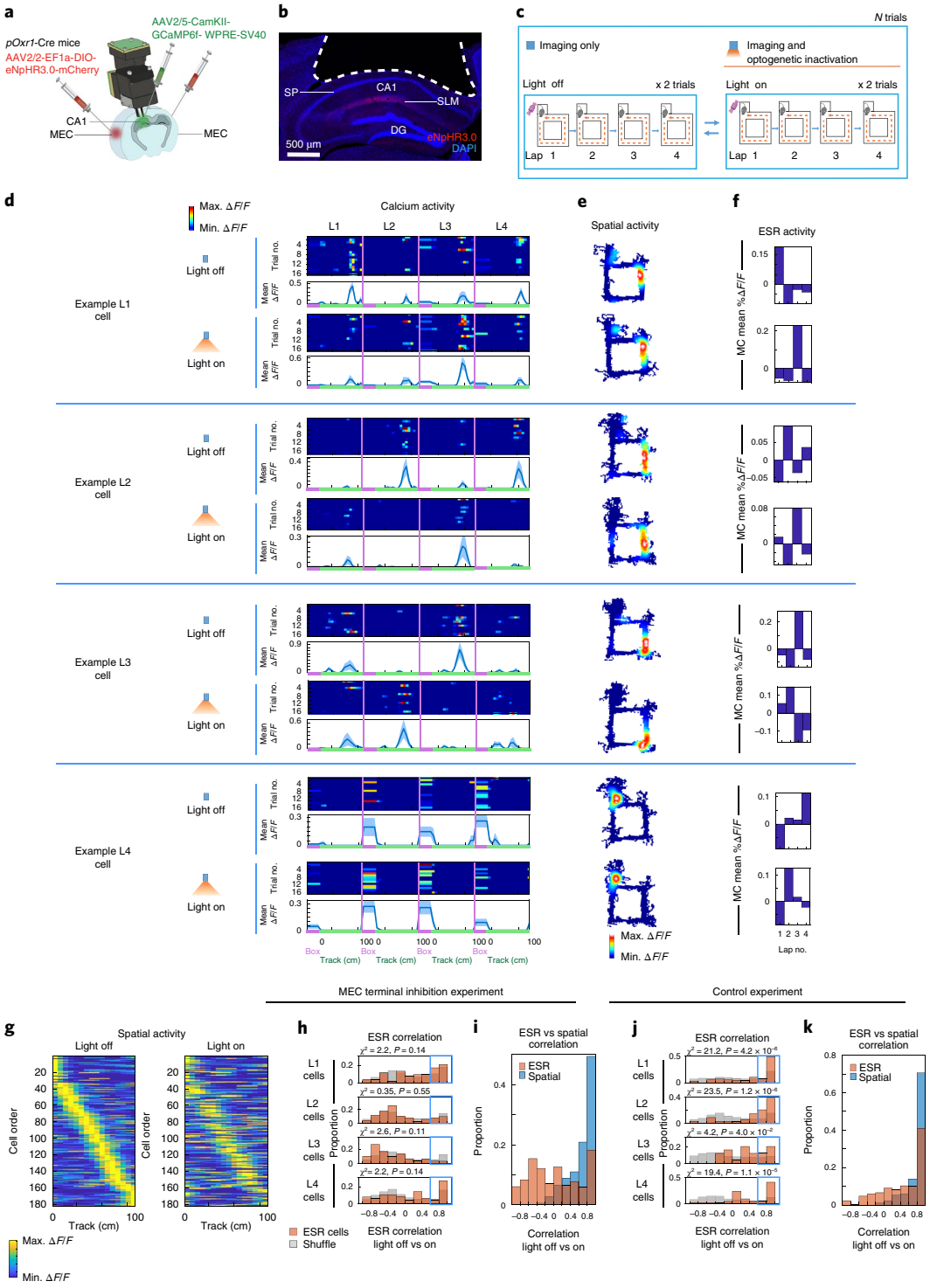

Fig. 6 | ESR activity and spatial activity are separately manipulable. a, Schematic of CA1 imaging and MEC terminal inhibition in the CA1, which were simultaneously conducted. **b**, An image of a coronal section of hippocampus showing the area of cortex aspiration (white dotted line) and MEC inputs labeled with eNpHR3.0 (red). DG, dentate gyrus; SLM, stratum lacunosum moleculare; SP, stratum pyramidale. Image is representative of aspiration surgeries from $n = 6$ *pOxr1*-Cre mice. **c**, During the standard four-lap-per-trial experiment, optogenetics light-on and light-off conditions were alternated every two trials for a total of 32–40 trials. **d**–**f**, Lap-specific neurons for example laps 1, 2, 3 and 4 with trial-by-trial calcium activity (**d**), spatial activity (**e**) and ESR activity (**f**) matched across the light-off versus light-on trials. The number of trials for each cell is indicated in each panel in **d**. **g**, The calcium activity of individual ESR cells sorted by the spatial location on the track during day 1, with this cell order matched across days (182 ESR cells, $n = 3$ mice). **h**, ESR correlations of these individual cells across light-on versus light-off. The proportion of cells with highly preserved ESR patterns across conditions (Pearson's $r > 0.6$, outlined in the blue boxes) was not significantly different compared to shuffles. χ^2 and P values shown in the figure ($n = 182$ cells). **i**, Individual cells showed high spatial correlations while ESR representations were perturbed across light-on versus light-off conditions ($n = 182$ cells). **j**, ESR correlations across light-on versus light-off conditions for control mice injected with AAV2/2-EF1a-DIO-mCherry (164 ESR cells, $n = 3$ mice). **k**, Individual cells from these control mice showed high spatial correlations and ESR correlations across light-on versus light-off conditions ($n = 164$ cells).

Taken together, the lap-specific activity pattern (that is, ESR) is reciprocally and independently manipulable from spatial activity, although the two representations are jointly expressed in the same cells.

Discrete event-modulated activity occurs together with continuous non-spatial activity. ESR activity and spatial activity are jointly represented in the same cells. What happens when the main continuous changes in the experience are not spatial? To answer this question, we conducted another four-lap-per-trial experiment in which the first arm of the standard four-lap-per-trial maze was replaced by a treadmill (Fig. 7a). Animals ran for 12 s on the treadmill at 14 cm s^{-1} for every lap. Monitoring the activity of neurons on a treadmill obviates the necessity of model corrections for running speed and head direction changes (Fig. 1g) because they are nearly constant on the treadmill (Extended Data Fig. 9a,b). Consistent with previous studies[3,4], cells were active during this non-spatial treadmill period (Fig. 7b,d). During the period restricted to the treadmill, 20% of CA1 cells (243 out of 1,222 cells, $n = 5$ animals) had significantly lap-modulated activity (Fig. 7g; Methods; for examples, see Fig. 7e) that exhibited a systematic lap-modulated pattern that was robust across trials (Fig. 7f). The percentage of ESR cells was reduced when reward was given every lap (6% (42 out of 681 cells), $n = 3$ animals; Fig. 7h–j). These results indicate that the tracking of experiences by the hippocampus occurs in a joint manner with an event-specific representation along with a continuous variable-tracking representation, even when the continuous experience is primarily non-spatial in nature.

Discussion

ESR tracks discrete units of experience. While mice ran a four-lap-per-reward task, approximately 30% of individual CA1 pyramidal neurons exhibited calcium activity levels that were significantly higher during one of the four laps. This ESR activity tracked the identities of laps despite variations in the duration needed to cover the lap events (Extended Data Fig. 8a,b) and even when pseudorandom variations in distance traveled were introduced during lap events (Fig. 3a–f). Therefore, ESR activity treats lap events as separate event units that are unaffected by spatiotemporal variations within current or neighboring events. In CA1 pyramidal cells, the ESR activity and spatial activity are jointly represented, so CA1 cells are active at a particular spatial field on the maze at a differential activity rate. But ESR activity tracks the lap identity even when this spatial field of CA1 cells was moved to an arbitrary location on a different maze (Fig. 4). Taken together, this shows that ESR treats different locations of a particular lap as part of the same event unit. When ESR was changed, it changed as a discrete, lap-specific shift rather than gradually through the course of the task experience (Fig. 5e,f: laps 1 and 2 not shifted versus laps 3 and 4 shifted).

Our finding of the ESR phenomenon is consistent with the theoretically derived concept[36,37], and with data obtained from human imaging studies[6–9,13], that alongside codes tracking continuous changes in spatial and sensory content, the brain tracks an experience by identifying one discrete unitary event after another as the entire experience progresses. These previous studies showed the involvement of the brain in event segmentation by showing heightened blood-oxygen-level-dependent activity at the boundaries between events[9], an observation that was recently confirmed by electrophysiology experiments[17]. Our present study provides further insight into the encoding of events by identifying a representation within single cells (ESR activity) that is tuned to the event units themselves rather than solely the event boundaries. ESR activity treats these events as fundamental units that make up the experience; therefore, they could be part of the neurophysiological basis for encoding events by the brain.

ESR tracks abstract, relational features of events and could support transfer learning. Recent human imaging and computational studies[10–13], including a computational model termed the "Eichenbaum–Tolman machine"[38], have suggested that the hippocampus is involved in coding the abstract structure that constitutes an episodic experience. Consistent with these studies, our present work, at the single-cell level, suggests a hippocampal activity pattern (the ESR) that not only tracks events but also tracks these events as putatively abstract entities. Indeed, our results show that the ESR consistently tracked lap events, irrespective of concrete sensory and spatiotemporal variations within the events (Figs. 3 and 4; Extended Data Figs. 8 and 10). Furthermore, ESR tracks the abstract and iterative relationships between events. In fact, we showed that ESR activity reliably distinguished the four lap events that were materially identical to one another but differed in their iterative and ordered relationships to the preceding and succeeding lap numbers (Fig. 1f,h). It is possible that the ESR differentially represents the four laps simply because it represents an internal variable like the gradually increasing level of motivation for acquiring another reward[39]. However, this is unlikely for two reasons. First, ESR activity patterns were not affected by arbitrary variations in the time and traveled distance required to complete the trial and receive reward (Fig. 3). Even during LLLL sequence trials, which were presented to the animal in an unpredictable fashion and the animal had to run on a maze length that was twice as long as the standard maze to reach the reward (Fig. 3e), the ESR activity patterns remained lap specific. Second, when an additional fifth lap was added to every trial in the task, lap 3 and 4 cells changed their activity on their respective lap, and shifted their activity by precisely one lap unit (Fig. 5d–l). This result suggests that ESR cells differentiate between the lap numbers

Fig. 7 | Discrete ESR activity occurs together with continuous non-spatial activity. a, Schematic of the four-lap-per-trial experiment with a 12-s treadmill period on each lap. ESR activity in this experiment was only investigated during the treadmill period. **b**, CA1 calcium activity sorted by time (s) of activity on the treadmill; the lap number showed activity at the same time on every lap, but displayed a higher activity level during a specific lap compared with other laps (222 cells from an example animal shown). **c**, Cartoon of mouse running during the treadmill period. The maze and door were not transparent in the task, but are shown as transparent here for illustration of the treadmill below. **d**,**e**, Trial-by-trial calcium activity of example neurons that did not have lap preference (**d**) and lap-specific neurons (**e**) for example laps 1, 2, 3 and 4. The top panels show trial-by-trial calcium activities, while the bottom panels show trial-averaged calcium activities (mean ± s.e.m.). The number of trials for each cell is indicated in each panel. The standard error was cut off at 0 because negative activity does not exist. **f**, ESR correlations between even numbered trials versus odd numbered trials of individual ESR cells (243 cells, $n = 5$ mice) as an indicator for preservation between trials within the session. The proportion of cells with highly preserved ESR patterns across trials (Pearson's $r > 0.6$, outlined in the blue boxes) was significantly greater compared to shuffles. **g**, Summary statistics of the percentage of ESR cells in the entire CA1 pyramidal population that were tuned to lap 1, 2, 3 or 4 in the 4-lap treadmill experiment (1,222 cells, $n = 5$ mice). **h**, For this task schedule, a reward was given to the animal following every lap. Every lap contained a 12-s treadmill period. **i**, The percentage of significant ESR cells was significantly higher during the four-lap-per-trial task (147 out of 696 cells) compared with the same animals during the reward every lap task (42 out of 681 cells), all during the treadmill period ($\chi^2 = 65.0$, $P = 7.8 \times 10^{-16}$, blue lines represent 3 mice). **j**, Summary statistics of the percentage of ESR cells in the entire CA1 pyramidal population that were tuned to lap 1, 2, 3 or 4 during the reward every lap experiment during the treadmill period (681 cells, $n = 3$ mice). ***$P < 0.001$.

as the animal's running progresses, and reflects the precise knowledge that lap 4 is no longer rewarded and that a fifth counted lap is now necessary to receive a reward. Altogether, our results indicate that ESR tracks the skeletal structure of experience via events as abstract entities, with abstract relationships between them.

In real life, there are few truly novel experiences, and most new experiences share either physical or abstract features with past experiences[10,12,28,40,41]. Learning a new task is improved through the transfer of knowledge from the web of related tasks that have already been learned, a phenomenon called "transfer learning"[42–45]. ESR appears

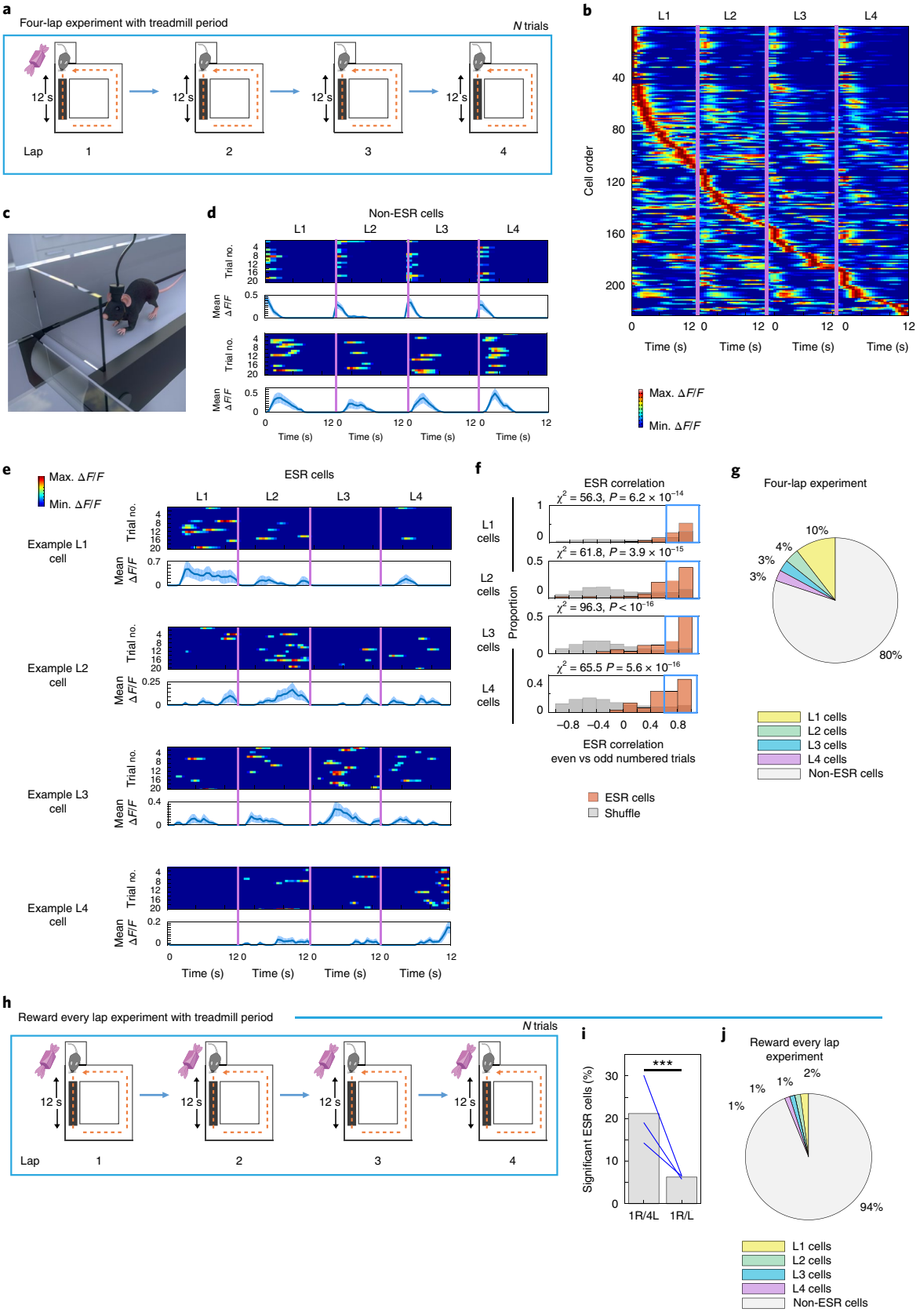

to track the events as abstract units and their abstract relationships; therefore, it may facilitate the transfer of knowledge between experiences that share these abstract features even if concrete spatial and sensory stimuli are distinct. Indeed, when the geometry of the maze was shifted from square to circular under the four-laps-per-reward conditions (Fig. 4), ESR activity was significantly maintained (Fig. 4f,d,g (orange histogram)) across these different experiences, even though place-field activity was globally remapped (Fig. 4c,e,g (blue histogram)). ESR activity could therefore capture not only the abstract structure within an experience (Figs. 1d and 3a–f) but also provides the elements (events) that can be reused during a different experience (Fig. 4).

ESR activity is independently manipulable from continuous spatial activity. Previous studies demonstrated that hippocampal cells change their firing rate in a particular spatial field in response to broader experiential changes, including sensory cues and past and future trajectory changes[1,4,14–16,18,46–49]. This has been termed "rate remapping". Consistent with these studies, ESR also showed a pattern of rate remapping (Fig. 1e) within the confines of the standard four-lap task.

Yet, ESR activity possessed an additional property: the pattern of rate remapping (that is, ESR activity) was maintained (Fig. 4g) even when the place-field location was moved to a new spatial location. These data indicate that ESR is not tied to a particular place-field location. In a reciprocal manner, ESR activity patterns could also be perturbed without a concomitant perturbation of spatial activity patterns, for instance, by the addition of a lap to the task (Fig. 5f) and by optogenetically inhibiting incoming MEC fibers (Fig. 6). The influence of ESR activity on neuronal activity is therefore mechanistically separate from the influence of spatial activity. Together, these results demonstrate that ESR activity is reciprocally and independently manipulable from spatial activity without affecting each other.

What are the benefits of tracking experience in a joint manner with both discrete and continuous representations? In fact, the two neural representations track different aspects of the same episodic experience. The tracking of immediate experience within an event likely requires a level of detail that would be best served by a continuous (spatial or non-spatial) neural representation. Conversely, tracking extended experience in a compact, flexible and generalizable way likely requires a level of abstraction above the moment-to-moment variational details and may be best served by encoding discrete and abstract event units. Ultimately, we found that ESR activity tracks events as fundamental units, is transferable between different experiences and is independently manipulable from continuous spatial activity. We propose that it might therefore constitute an independent code from the spatial code: an 'event code' that is dedicated to tracking events as discrete units of experience, alongside codes monitoring continuously changing variables. This event code may help the brain track experience in an efficient and flexible manner.

Online content

Any methods, additional references, Nature Research reporting summaries, source data, extended data, supplementary information, acknowledgements, peer review information; details of author contributions and competing interests; and statements of data and code availability are available at https://doi.org/10.1038/s41593-020-0614-x.

Received: 27 August 2019; Accepted: 20 February 2020;
Published online: 6 April 2020

References

1. Sakurai, Y. Coding of auditory temporal and pitch information by hippocampal individual cells and cell assemblies in the rat. *Neuroscience* **115**, 1153–1163 (2002).
2. O'Keefe, J. & Dostrovsky, J. The hippocampus as a spatial map. Preliminary evidence from unit activity in the freely-moving rat. *Brain Res.* **34**, 171–175 (1971).
3. MacDonald, C. J., Lepage, K. Q., Eden, U. T. & Eichenbaum, H. Hippocampal "time cells" bridge the gap in memory for discontiguous events. *Neuron* **71**, 737–749 (2011).
4. Pastalkova, E., Itskov, V., Amarasingham, A. & Buzsaki, G. Internally generated cell assembly sequences in the rat hippocampus. *Science* **321**, 1322–1327 (2008).
5. Aronov, D., Nevers, R. & Tank, D. W. Mapping of a non-spatial dimension by the hippocampal–entorhinal circuit. *Nature* **543**, 719–722 (2017).
6. Schapiro, A. C., Rogers, T. T., Cordova, N. I., Turk-Browne, N. B. & Botvinick, M. M. Neural representations of events arise from temporal community structure. *Nat. Neurosci.* **16**, 486–492 (2013).
7. Richmond, L. L. & Zacks, J. M. Constructing experience: event models from perception to action. *Trends Cogn. Sci.* **21**, 962–980 (2017).
8. Ben-Yakov, A. & Henson, R. N. The hippocampal film editor: sensitivity and specificity to event boundaries in continuous experience. *J. Neurosci.* **38**, 10057–10068 (2018).
9. Zacks, J. M. et al. Human brain activity time-locked to perceptual event boundaries. *Nat. Neurosci.* **4**, 651–655 (2001).
10. Friston, K. & Buzsaki, G. The functional anatomy of time: what and when in the brain. *Trends Cogn. Sci.* **20**, 500–511 (2016).
11. Hard, B. M., Tversky, B. & Lang, D. Making sense of abstract events: building event schemas. *Mem. Cognit.* **34**, 1221–1235 (2006).
12. Schank, R. C. & Abelson, R. P. *Scripts, Plans, Goals and Understanding: An Inquiry into Human Knowledge Structures* (L. Erlbaum, 1977).
13. Baldassano, C. et al. Discovering event structure in continuous narrative perception and memory. *Neuron* **95**, 709–721 (2017).
14. Leutgeb, S. et al. Independent codes for spatial and episodic memory in hippocampal neuronal ensembles. *Science* **309**, 619–623 (2005).
15. Wood, E. R., Dudchenko, P. A., Robitsek, R. J. & Eichenbaum, H. Hippocampal neurons encode information about different types of memory episodes occurring in the same location. *Neuron* **27**, 623–633 (2000).
16. Frank, L. M., Brown, E. N. & Wilson, M. Trajectory encoding in the hippocampus and entorhinal cortex. *Neuron* **27**, 169–178 (2000).
17. Bulkin, D. A., Sinclair, D. G., Law, L. M. & Smith, D. M. Hippocampal state transitions at the boundaries between trial epochs. *Hippocampus* https://doi.org/10.1002/hipo.23180 (2019).
18. Terada, S., Sakurai, Y., Nakahara, H. & Fujisawa, S. Temporal and rate coding for discrete event sequences in the hippocampus. *Neuron* **94**, 1248–1262 (2017).
19. Wood, E. R., Dudchenko, P. A. & Eichenbaum, H. The global record of memory in hippocampal neuronal activity. *Nature* **397**, 613–616 (1999).
20. Chen, T. W. et al. Ultrasensitive fluorescent proteins for imaging neuronal activity. *Nature* **499**, 295–300 (2013).
21. Kitamura, T. et al. Island cells control temporal association memory. *Science* **343**, 896–901 (2014).
22. Okuyama, T., Kitamura, T., Roy, D. S., Itohara, S. & Tonegawa, S. Ventral CA1 neurons store social memory. *Science* **353**, 1536–1541 (2016).
23. Ziv, Y. et al. Long-term dynamics of CA1 hippocampal place codes. *Nat. Neurosci.* **16**, 264–266 (2013).
24. Czurko, A., Hirase, H., Csicsvari, J. & Buzsaki, G. Sustained activation of hippocampal pyramidal cells by 'space clamping' in a running wheel. *Eur. J. Neurosci.* **11**, 344–352 (1999).
25. McNaughton, B. L., Barnes, C. A. & O'Keefe, J. The contributions of position, direction, and velocity to single unit-activity in the hippocampus of freely-moving rats. *Exp. Brain Res.* **52**, 41–49 (1983).
26. Leutgeb, S., Ragozzino, K. E. & Mizumori, S. J. Y. Convergence of head direction and place information in the CA1 region of hippocampus. *Neuroscience* **100**, 11–19 (2000).
27. O'Keefe, J. & Nadel, L. *The Hippocampus as a Cognitive Map* (Clarendon Press, 1978).
28. Behrens, T. E. J. et al. What is a cognitive map? Organizing knowledge for flexible behavior. *Neuron* **100**, 490–509 (2018).
29. Hahn, T. T. G., McFarland, J. M., Berberich, S., Sakmann, B. & Mehta, M. R. Spontaneous persistent activity in entorhinal cortex modulates cortico–hippocampal interaction in vivo. *Nat. Neurosci.* **15**, 1531–1538 (2012).
30. Robinson, N. T. M. et al. Medial entorhinal cortex selectively supports temporal coding by hippocampal neurons. *Neuron* **94**, 677–688 (2017).
31. Miao, C. et al. Hippocampal remapping after partial inactivation of the medial entorhinal cortex. *Neuron* **88**, 590–603 (2015).
32. Tsao, A. et al. Integrating time from experience in the lateral entorhinal cortex. *Nature* **561**, 57–62 (2018).
33. Ito, H. T., Zhang, S. J., Witter, M. P., Moser, E. I. & Moser, M. B. A prefrontal–thalamo–hippocampal circuit for goal-directed spatial navigation. *Nature* **522**, 50–55 (2015).

34. Suh, J., Rivest, A. J., Nakashiba, T., Tominaga, T. & Tonegawa, S. Entorhinal cortex layer III input to the hippocampus is crucial for temporal association memory. *Science* **334**, 1415–1420 (2011).
35. Yamamoto, J., Suh, J., Takeuchi, D. & Tonegawa, S. Successful execution of working memory linked to synchronized high-frequency gamma oscillations. *Cell* **157**, 845–857 (2014).
36. Zacks, J. M., Speer, N. K., Swallow, K. M., Braver, T. S. & Reynolds, J. R. Event perception: a mind/brain perspective. *Psychol. Bull.* **133**, 273–293 (2007).
37. Tulving, E. *Organization of Memory* (Academic Press, 1972).
38. Whittington, J. C. et al. The Tolman–Eichenbaum machine: unifying space and relational memory through generalisation in the hippocampal formation. Preprint at *bioRxiv* https://doi.org/10.1101/770495 (2019).
39. Gauthier, J. L. & Tank, D. W. A dedicated population for reward coding in the hippocampus. *Neuron* **99**, 179–193 (2018).
40. Dragoi, G. & Tonegawa, S. Preplay of future place cell sequences by hippocampal cellular assemblies. *Nature* **469**, 397–401 (2011).
41. Foster, D. & Wilson, M. Reverse replay of behavioural sequences in hippocampal place cells during the awake state. *Nature* **440**, 680–683 (2006).
42. Pratt, L. Y. Discriminability-based transfer between neural networks. *Adv. Neural Info. Process. Sys.* **5**, 204–211 (1992).
43. Tse, D. et al. Schemas and memory consolidation. *Science* **316**, 76–82 (2007).
44. Hinton, G. E. in *Parallel Distributed Processing: Implications for Psychology and Neurobiology* (ed. Morris, R. G. M.) 46–61 (Clarendon Press/Oxford Univ. Press, 1989).
45. Yosinski, J., Clune, J., Bengio, Y. & Lipson, H. How transferable are features in deep neural networks? *Advances in Neural Information Processing Systems* **27**, 3320–3328 (2014).
46. Spiers, H. J., Hayman, R. M., Jovalekic, A., Marozzi, E. & Jeffery, K. J. Place field repetition and purely local remapping in a multicompartment environment. *Cereb. Cortex* **25**, 10–25 (2015).
47. Grieves, R. M., Jenkins, B. W., Harland, B. C., Wood, E. R. & Dudchenko, P. A. Place field repetition and spatial learning in a multicompartment environment. *Hippocampus* **26**, 118–134 (2016).
48. Derdikman, D. et al. Fragmentation of grid cell maps in a multicompartment environment. *Nat. Neurosci.* **12**, 1325–1332 (2009).
49. Singer, A. C., Karlsson, M. P., Nathe, A. R., Carr, M. F. & Frank, L. M. Experience-dependent development of coordinated hippocampal spatial activity representing the similarity of related locations. *J. Neurosci.* **30**, 11586–11604 (2010).

Methods

Animals. All procedures relating to mouse care and treatment conformed to the Massachusetts Institute of Technology's Committee on Animal Care guidelines and NIH guidelines. Animals were individually housed in a 12-h light (19:00–7:00)–dark cycle. Twenty-four male *Wfs1*-Cre mice aged between 2 and 4 months were implanted with an Inscopix microendoscope into the CA1 and food was restricted to 85–90% normal body weight for the experiments. For each of the six main maze-manipulation imaging experiments (random maze elongation experiment, circular maze experiment, lap addition experiment, treadmill experiment, fixed maze elongation experiment and spatial alternation experiment), the number of animals used (at least four) is indicated in the main text for each experiment. In each of these experiments, at least two of these tested animals did not previously undergo any of the other manipulative experiments. The other animals were experienced animals from the other manipulative experiments. Significant ESR cells were found during each of these maze manipulation sessions (Supplementary Figs. 2 and 3). Six *pOxr1*-Cre mice (three for the MEC terminal inhibition experiment and three control mice), aged 2–4 months, were also implanted with an Inscopix microendoscope into the CA1 for dual imaging and optogenetics experiments, and were trained in a same manner as the *Wfs1*-Cre mice.

Histology and immunohistochemistry. Mice were transcardially perfused with 4% paraformaldehyde in PBS. Brains were then post-fixed with the same solution for 24 h, and brains were sectioned using a vibratome. Sections were stained using 4,6-diamidino-2-phenylindole (DAPI). Micrographs were obtained using a Zeiss AxioImager M2 confocal microscope and Zeiss ZEN (black edition) software.

Preparation of AAVs. The AAV2/5-Syn-flex-GCaMP6f-WPRE-SV40 was generated by and acquired from the University of Pennsylvania Vector Core, with a titer of 1.3×10^{13} genome copies per ml. The AAV2/5-CamKII-GCaMP6f-WPRE-SV40 was generated by and acquired from the University of Pennsylvania Vector Core, with a titer of 2.3×10^{13} genome copies per ml. The AAV2/2-EF1a-DIO-eNpHR3.0-mCherry was generated by and acquired from the University of North Carolina (Chapel Hill) Vector Core, with a titer of 5.3×10^{12} genome copies per ml.

Stereotactic surgery. Stereotactic viral injections and microendoscope implantations were all performed in accordance with Massachusetts Institute of Technology's Committee on Animal Care guidelines. Mice were anesthetized using 500 mg per kg of avertin. Viruses were injected using a glass micropipette attached to a 10-µl Hamilton microsyringe through a microelectrode holder filled with mineral oil. A microsyringe pump and its controller were used to control the speed of the injection. The needle was slowly lowered to the target site and remained for 10 min after the injection.

For CA1 imaging experiments, unilateral viral delivery into the right CA1 of the *Wfs1*-Cre mice was aimed at the following coordinates relative to Bregma: anterior–posterior (AP): −2.0 mm; medial–lateral (ML): +1.4 mm; and dorsal–ventral (DV): −1.55 mm. *Wfs1*-Cre mice were injected with 300 nl of AAV2/5-Syn-flex-GCaMP6f-WPRE-SV40. Approximately 1 month after injection, a microendoscope was implanted into the dorsal part of the CA1 of the *Wfs1*-Cre mice aimed at the following coordinates relative to Bregma: AP: −2.0 mm; ML: +2.0 mm; and DV: approximately −1.0 mm. To implant at the correct depth, the cortex was vacuum-aspirated, resulting in the removal of the corpus callosum, which is visible under a surgical microscope as fibers running in the ML direction. The fibers of the alveus, which are visible as fibers running in the AP direction, were left intact by the procedure.

For CA1 optogenetic and imaging experiments, 300 nl of AAV2/5-CamKII-GCaMP6f- WPRE-SV40 was unilaterally delivered into the right CA1 of *pOxr1*-Cre mice using the following coordinates relative to Bregma: AP: −2.0 mm; ML: +1.4 mm; and DV: −1.55 mm. Also, 300 nl of AAV2/2-EF1a-DIO-eNpHR3.0-mCherry was bilaterally delivered into the MEC of these mice using the following coordinates relative to Bregma: AP: −4.85 mm; ML: ±3.45 mm; and DV: −3.35 mm. Control *pOxr1*-Cre mice received the same CA1 viral delivery and received a bilateral delivery into MEC, but the bilaterally delivered virus was the control virus AAV2/2-EF1a-DIO-mCherry. Following these virus injections, the microendoscopy lens was implanted in the same manner as for the dual optogenetic and imaging experiments, as described above for the CA1 imaging experiments.

The baseplate for the miniaturized microscope camera was attached above the implanted microendoscope in the mice. After experiments, animals were perfused, and post hoc analyses were examined to determine the actual imaging position in the CA1 (Figs. 1c and 6b).

Apparatus description and experimental conditions. The apparatus was a square maze 25 cm in length and width, with a 5-cm-wide track width, and 7 cm in height. A 10 cm × 10 cm square reward box was located in one corner of the square maze. Sugar pellets (Bio-Serve, F5684) were placed in the reward box at the beginning of lap 1 of each trial. Four versions of this apparatus were used. Version 1 was used in Figs. 1,2,5 and 6. Version 2 used in Fig. 3 had a length elongation that was twice the standard length (50 cm = 2 × 25 cm), but was otherwise identical to Version 1 in other dimensions. Version 3, used in the treadmill experiment (Fig. 7), had a 18-cm-long treadmill installed in the arm of the maze that immediately faces the reward box (Fig. 7a). Version 3 otherwise used the same dimensions as Version 1. Version 4, used in Extended Data Fig. 10, had an eight-maze configuration, with the other square of the eight-maze being 25 cm in length and width. Version 4 otherwise used the same dimensions as Version 1. The circular maze, used in Fig. 4, was constructed to have the same total path length (that is, circumference) as the Version 1 square maze, and the same reward box size. All mazes were opaque and black.

All maze experiments were performed under dim light conditions, with prominent visual cues within 50 cm on all sides of the box. Ca^{2+} imaging in the maze lasted at least 20 min to collect a sufficient number of Ca^{2+} transients to power our statistical analyses. The maze surface was cleaned between sessions with 70% ethanol. Immediately before and after imaging sessions, the mouse rested on a pedestal next to the maze.

The basic task used in this manuscript was the standard four-lap-per-trial task, whereby animals traversed round a square maze 25 cm in length (1 m journey in total) (Fig. 1d). The task was designed so that a sugar pellet reward was delivered manually to the reward box at the beginning of lap 1 once every 4 such laps, which we call a single trial (Fig. 1d). Identical motions were made on each lap, regardless of whether a pellet was delivered. During the testing phase, animals completed 15–20 of such trials in repetitive succession without interruption. For any behavioral session in which the animal missed going into the reward box more than once in the entire sequence of runs (15–20 × 4 = 60–80 runs in total), the experiment was excluded. Crucially, for all experiments, animals first underwent task training before the final testing days. Training procedures are described below.

Habituation to reward in the maze. All behavior experiments took place during the dark cycle of the animals. All implanted mice were habituated to human experimenters and the experimental room. At the same time, they were mildly food-restricted and habituated to the sugar pellet reward. The criterion for habituation to sugar pellets and the maze was running counter-clockwise around the maze and eating a sugar pellet in the reward port of the maze (described below) in 15 successive repetitions without missing a single pellet.

Reward periodicity training. Animals were trained for approximately 8 days. If during any training day the mice appeared unmotivated or too satiated to complete the 15 trials, that training day was repeated the following day. Animals were pretrained for 2 days on the maze to habituate to receiving sugar pellet rewards in the reward port: on each of these days, they did a one-lap-per-trial task; that is, they received a reward after every run around the maze, and ran 15 such trials. For the next 3 days (days 3–5), animals were trained to receive periodic rewards. On day 3, animals ran 15 trials of a 2-lap-per-trial task; that is, they received reward every 2 laps around the maze. On day 4, animals ran 15 trials of a 3-lap-per-trial task. On day 5, animals ran 15 trials of a 4-lap-per-trial task. Finally, animals ran 3 more days (days 6–8), 15 trials per day of a 4-lap-per-trial task, before they were considered well trained on the basic 4-lap-per-trial task.

Untrained versus well-trained experiment protocol. In the particular case of the untrained versus well-trained animal experiment (Extended Data Fig. 4c–e), animals that had only been habituated to the reward (described above) were immediately tested and imaged by running 15 trials of the standard 4-lap-per-trial task. Following this initial testing, these animals then underwent the reward periodicity training (described above). Following periodicity training, animals were tested and imaged again for 15 trials of the standard 4-lap-per-trial task to compare ESR cells seen after training compared with when they were untrained.

Reward on every lap experiment. Animals in this experiment (Figs. 1i–k and 5a–c) were given a sugar pellet on every lap and completed a total of 60–80 laps total. This is equivalent to the total number of laps in the 15–20 trials of the 4 lap-per-trial experiment. This experiment did not require extra or task-specific training.

Task-specific training. Each of the main maze-manipulation experiments (random maze elongation experiment, circular maze experiment, lap addition experiment, treadmill experiment, fixed maze elongation experiment and spatial alternation experiment) required its own special task training after completing the habituation and reward periodicity training.

Random maze elongation experiment. For the random maze elongation experiment (Fig. 3), animals were tested and imaged on 28 4-lap trials. The maze was manually elongated on pseudorandom laps of random trials using detachable walls, such that each of the four types of trials (SSSS, SSLL, LLSS and LLLL, where S denotes a short lap and L denotes a long lap) were presented in a pseudorandom order and appeared 7 times each within the 28 trials. The entire 28 consecutive sequence of trials was as follows: SSSS, LLSS, LLLL, SSSS, SSSS, SSLL, SSLL, LLSS, LLLL, LLSS, LLSS, SSLL, LLLL, LLLL, SSSS, LLLL, LLLL, LLSS, LLLL, LLSS, SSSS, LLSS, SSLL, SSSS, SSSS, SSLL, SSLL, SSLL. Before the test day, animals underwent 3 days (days −3 to −1) of habituation training to the short and long laps, where SSSS, SSLL, LLSS and LLLL trials were randomly presented.

Circular maze experiment. For the circular maze experiment (Fig. 4), animals were tested and imaged in a 2-day experiment. These animals underwent 3 days (days −3 to −1) of habituation training before the first test day. On the first two training days (days −3 to −2), animals ran 15 trials on the circular maze each day. On the third day of training (day −1), animals ran 15 trials on the square maze again to get them habituated to the test day. On each of the test days, 1 h before experimentation, animals ran on the maze for five four-lap-per-reward trials.

Five-lap-per-trial experiment. For the five-lap-per-trial experiment (Fig. 5), animals were tested and imaged in a 2-day experiment. These animals underwent 3 days (days −3 to −1) of habituation training before the first test day. On the first two training days (days −3 to −2), animals each day ran 15 trials of a 5-lap-per-trial task. On the third day of training (day −1), animals ran 15 trials of a 4-lap-per-trial task again to get them habituated to the test day.

Optogenetics experiment. Calcium imaging used the Inscopix nVoke miniature optoscope at 20 Hz. During periods of optogenetic manipulation, as defined by our protocol (Fig. 6c), the Inscopix nVoke miniature optoscope's orange light (590–650 nm) stimulation was turned on at 10 mW mm^{-2} power at a uniform and constant level. Orange light delivery was manually performed and was turned on or off at the start of the relevant trial as soon as animals entered the box.

For the optogenetics manipulation experiment, animals were tested and imaged in a single day. These animals underwent 2 days of habituation training before the first test day, with 2 days in between each of the training days to allow recovery from the light. On each of the training days, animals ran 16 trials each day of a 4-lap-per-trial task with the light schedule according to the alternating schedule shown in Fig. 6c.

Treadmill experiment. For the treadmill experiment (Fig. 7), animals were tested and imaged in a single day. These animals underwent 6 days of habituation training running on the maze before the first test day. On the first day of training, animals ran 15 trials of a 1-lap-per-trial task. During each lap, the animal ran onto the first arm of the square maze and ran for 12 s (time period accurately indicated via Arduino, and manually initiated) on the treadmill at a constant 14 cm s^{-1}, before running around the rest of the square maze and entering the reward box. On the next 5 days of training, animals ran 15 trials of a 4-lap-per-trial task again with 12 s on the treadmill to get them habituated to the test day.

Fixed maze elongation experiment. For the fixed maze elongation experiments (Extended Data Fig. 8), animals were tested and imaged in a 2-day experiment. On day 2, 2 h before experimentation, animals were habituated (allowed to run) for 3 min on the distorted maze without any rewards.

Alternation maze experiment. For the spatial alternation experiment, animals were tested and imaged in a 2-day experiment. These animals underwent 5 days (days −5 to −1) of habituation training before the first test day. On the first four training days (days −5 to −2), animals ran 15 trials each day of a 4-lap-per-trial task, whereby the laps alternated in their spatial trajectories as shown in Extended Data Fig. 10a. Path alternation was manually induced in the maze using detachable walls. On the fifth day of training (day −1), animals underwent 15 trials of an ordinary (non-alternating) 4-lap-per-trial task again to get them habituated to the test day.

Behavioral analysis and Ca^{2+} events detection. The position of the animal was captured using an infrared camera (Ordro infrared camcorder, 30 frames per second) via infrared light-emitting diodes (LEDs) attached to the animal. Calcium events were captured at 20 Hz on an Inscopix miniature microscope. Imaging sessions were time stamped to the start of the behavioral recording session by turning on an LED that was fixed to the animal at the beginning of the session and turning off the LED at the end.

Analyses of the calcium images and extraction of independent neuronal traces were done as previously described[23,50]. Specifically, the calcium images were binned four times spatially along each dimension and then processed using custom-made code written in ImageJ (dividing each image, pixel-by-pixel, using a low-passed (r = 20 pixels) filtered version). It was then motion-corrected in Inscopix Mosaic software 1.2.0 (correction type: translation and rotation; reference region with spatial mean (r = 20 pixels) subtracted, inverted and spatial mean applied (r = 5 pixels)). A spatial mean filter was applied in Inscopix Mosaic (disk radius = 3), and a $\Delta F/F$ signal was calculated.

Four hundred putative region of interest (ROI) locations were selected from the resulting movie using principal component (PC) analysis (PCA) and independent component (IC) analysis (ICA) (600 output PCs, 400 ICs, 0.1 weight of temporal information in spatiotemporal ICA, 750 iterations maximum, 1E-5 fractional change to end iterations) in Inscopix Mosaic software. ROIs, half-max thresholded, that were not circular (if its length exceeded its width by >2.5 times) or smaller than 5 pixels in diameter (~12 μm) were discarded. For each remaining ROI (that is, a putative neuron), pixels within the ROI filter that were <75% of the filter's maximum intensity were zeroed. ROIs in the same session that were closer than 3 pixels (~7 μm) were considered the same cell rather than different cells.

$\Delta F/F$ calcium traces were calculated for the resulting ROI filters for each processed movie. Slow variations in the calcium traces were eliminated by subtracting the median percentile $\Delta F/F$ value at each timepoint value calculated from the calcium trace values ±15 s within this timepoint, similar to a previously described method[23]. The calcium trace was smoothed by four temporal bin-rolling averages (50 ms for each bin). Significant calcium transients (Fig. 1c) were defined as traces that exceeded three standard deviations above baseline and remained above 1.5 standard deviations above baseline for at least 500 ms. The rest of the $\Delta F/F$ calcium traces, aside from its significant transients, were zeroed in a similar way to a previously described method[51]. The decay time of all calcium transients across n = 14 animals was calculated, and the median decay time (the time required for a calcium transient to decay to half its maximum height) of these 137,045 calcium events was 1.35 s (Extended Data Fig. 2a). Only cells that had a total of at least 25 significant transients during the entire session and non-zero activity in at least 10 trials separately were considered for further analysis in this study. In the sole case of the treadmill experiment, a lesser total of at least 10 significant transients was used since the cumulation of all the treadmill periods was only 12–16 min (15–20 trials).

ESR cell calculation. *Calcium event filtering.* For each CA1 cell detected, the calcium activity was filtered so that only activity occurring while the mice were in an active state (animal speed > 4 cm s^{-1}) were further analyzed. The behaviorally tracked times of interest were also filtered in this way, considering only the times when animal speed was >4 cm s^{-1}. The maze was divided into nine spatial bins: the reward box (spatial bin of length and width 10 cm) was one spatial bin, and each of the four arm lengths of the maze was divided in half (8 spatial bins, each of which was 12.5 cm in length and 5 cm in width).

Next, for each identified cell, individual calcium activity epochs were analyzed by calculating the mean calcium activity in each of the nine spatial bins during each individual lap across trials. Thus, for a session of 15–20 trials, there were 540–720 calcium activity epochs in total (15–20 × 9 × 4 = 540–720).

Each CA1 neuron possesses spatially tuning, and in this model, the spatial tuning was captured by a parameter p defined as the probability of having non-zero calcium activity in each separate spatial bin. The p was calculated for each neuron for each of its spatial bins. It differed for different spatial bins, which reflected the spatially modulated activities.

Linear model fitting. For each activity epoch for each neuron, the mean $\Delta F/F$ calcium activity, the mean speed (s) and the head direction tuning (o) were calculated. The non-zero calcium activity epochs were fit using a linear regression of the mean $\Delta F/F$ calcium activity versus speed and head direction tuning. In this regression, the coefficients a, b and c were fit as follows:

$$R[\mathrm{Ca}] \sim (a \times s + b \times o + c) \quad (1)$$

Where R[Ca] is the mean $\Delta F/F$ calcium activity level of this neuron during this activity epoch, s is the mean speed of the animal during this activity epoch and o is the head orientation deviation from the preferred head orientation of this neuron during this activity epoch. In Matlab code, we used the function fitrlinear with lambda = 0.01 to fit equation (1) using regularized linear regression applied to the calcium activity epochs of all cells.

Identification of ESR cells. For each identified cell, we shuffled its calcium transients across the lap epochs such that the probability of assigning any particular calcium transient into any particular lap epoch varied according to equation (1). Calcium transients were only shuffled (using randperm in Matlab) between different epochs taking place in the same spatial field to preserve p. We checked that this shuffle generation procedure gave a mean $\Delta F/F$ calcium activity level that matched the model-predicted (equation (1)) calcium activity level (Extended Data Fig. 2d). These shuffles simulated the calcium activity of the cell explained by spatial field (p), head direction (o) and animal speed (s). A total of 5,000 such shuffles were computed, and a 'model-explained mean $\Delta F/F$ calcium activity level' was computed as follows:

$$R_{\mathrm{model}}[\mathrm{Ca},\ L = i,\ S = j] = \mathrm{mean}(R[\mathrm{Ca},\ L = i,\ S = j])_{\mathrm{shuffles}}$$

Where R[Ca, $L = i$, $S = j$] is the model-explained calcium activity computed as the mean activity in lap i and spatial bin j across all the shuffles for this cell.

For every neuron for all four individual laps, the model-explained mean calcium activity level in each individual spatial bin was subtracted from the real mean $\Delta F/F$ calcium activity to yield the MC $\Delta F/F$ calcium activity, which excluded spatial, mean speed and mean head direction tuning (Fig. 1g). Thus, this MC effect would mainly reflect the difference in calcium activity due to lap number.

For every neuron, the model-explained mean $\Delta F/F$ calcium activity level was subtracted from the mean $\Delta F/F$ calcium activity level obtained from the 5,000 shuffles to yield a distribution of MC $\Delta F/F$ activities for chance level statistics. Cells whose peak, lap-specific MC $\Delta F/F$ was outside the 95th percentile confidence interval of shuffled MC $\Delta F/F$ were significant ESR cells.

If the peak MC calcium activity happened to occur during the reward-eating lap (lap 1) while the animal was in the reward box spatial bin, then the peak MC

calcium activity from the next highest spatial bin was selected because we excluded cell activity that was directly driven by reward eating.

Robustness of ESR phenomenon to different parameter choices. To show that our experimental results were not simply due to our model correction, we reexamined the maze variation experiments using the raw $\Delta F/F$ activity of these ESR cells rather than the MC $\Delta F/F$ activity. These experiments showed similar results to those obtained when model correction was done (Extended Data Fig. 6).

To further characterize the robustness of lap-specific activity across trials, an analysis of statistical power was conducted by randomly removing one-quarter of all trials (that is, four to five trials) during the standard four-lap experiment for each mouse. We note that 69% (726 out of 1,055) of previously statistically significant ESR cells retained their significance (Extended Data Fig. 3a, left). By comparison, within the previous subpopulation of non-ESR cells, 5% (131 out of 2,451) now showed significance within the error rate. Even with this one-quarter of trials removed, ESR activity was still well correlated across days (Extended Data Fig. 3a, center and right).

To examine whether results were affected by the spatial bin size that we used, we re-analyzed the standard four-lap experiment with a smaller spatial bin size, while keeping the rest of the procedures described above. We divided each of the four arm lengths into four equal bins (each 6.25 cm in length), and the box into four equal bins for a total of 20 spatial bins. We obtained nearly identical experimental results as that of nine spatial bins (Extended Data Fig. 3c), so we proceeded with utilizing nine spatial bins for the rest of the experiments.

To examine whether cells that showed lap-dependent activity were more generally stochastic, we looked at the subpopulation of ESR cells that had a higher consistency of activity, which we defined as cells that were active in the main spatial bin during at least half of all the trials. Again, this subpopulation of neurons had robustly preserved ESR activity across days during the standard four-lap experiment (Extended Data Fig. 3f).

Spatial information. The tracked positions were sorted into 16 spatial bins 6.25 cm × 5 cm in size around the track and 4 spatial bins 5 cm × 5 cm in size in the reward box, and the mean $\Delta F/F$ calcium activity of each CA1 cell was determined for each bin. The bins that had animal occupancy values of <100 ms were considered unreliable and discarded from further analysis. Without smoothing, the spatial tuning was calculated for each cell as follows:

$$\sum_i p_i \lambda_i \log_2 \frac{\lambda_i}{\lambda}$$

Where λ_i is the mean $\Delta F/F$ calcium activity of a unit in the i-th bin, λ is the overall $\Delta F/F$ calcium activity, and p_i is the probability of the animal occupying the i-th bin for all i. This formulation, derived from a previous study[52], was applied to calcium activity levels, which have a known monotonic relationship to spike rates[20]. All event times of cells were shuffled 2,000 times in an analogous manner to a previously described method[53] by shifting the calcium activity time series around the position data by a random translation of >20 s and less than the session duration minus 20 s. Cells with significant spatial information were determined above the 95th percentile of all shuffles.

Registering cells across days. Our approach to register cells across days was to do so on the basis of the anatomy of the field of view seen on both days (that is, the pattern of blood vessels, among other parameters), rather than directly on the spatial locations of cells (Extended Data Fig. 5a). To register two movies across days, a mean projection of the ImageJ-filtered and motion-corrected movie (see above) on each day was computed, and these two movies were registered with respect to one another using Inscopix Mosaic motion correction software. The distances between active cells from day 1 and their putatively matched cells on day 2 (650 cells, $n = 4$ animals) were calculated. The distribution of distances had a mode of 1.2 µm (Extended Data Fig. 5c, purple bars). By contrast, the distribution of distances between these same cells on day 1 and their nearest neighboring cells on the same day had a mode of 17.6 µm (Extended Data Fig. 5c, yellow bars).

After an appropriate image registration was found for the fields of view based on anatomy, the ROIs on day 1 were identified, and calcium traces were calculated based on the resulting ROI filters for day 1 applied directly to the processed movie on day 2 at the matching anatomical location. This is exactly what would have been done if the day 2 movie had been a part of day 1. We note that the resulting spatial fields of registered cells were preserved across days (Fig. 2f), which provides an independent validation of our cell registration protocol.

ESR activity and spatial activity correlations across days. For ESR correlations across days, for a given significant ESR cell on day 1, its ESR activity pattern (defined in the main text) was concatenated into a vector. A similar vector was produced for this same cell on day 2. This was done for each significant ESR cell defined on day 1. The ESR correlation acted as an index for ESR preservation across days and was defined as the Pearson's correlation between the day 1 ESR activity vector and the corresponding day 2 ESR activity vector for the same cell. The day 2 ESR activity vector was produced from the same spatial bin as day 1 to allow for direct comparisons of ESR activity, except for the circular maze and spatial trajectory alternation experiments. In these cases, the spatial bins in which peak activity occurred were calculated anew, since the space was substantially changed in these experiments relative to room cues.

ESR cells with Pearson's $r > 0.6$ threshold were considered to have highly preserved (that is, highly correlated) ESR activity patterns across days. The distribution of ESR correlations when cell identities were shuffled across days was bimodal (Extended Data Fig. 3d). Since we required a measure for shuffled cell pairs that were highly correlated by chance, we chose the threshold $r > 0.6$, which marks the boundary to the mode at $r = 1$. With other choices of threshold, $r > 0.4$ or $r > 0.8$, all the subpopulations of lap 1–4 cells separately were still highly preserved during the 2-day standard 4-lap task (Extended Data Fig. 3e).

For spatial correlations across days, the raw calcium events, speed filtered (>4 cm s^{-1}), were sorted into the nine spatial bins defined above, the calcium activity level of each neuron was determined for each bin, and an activity map composed of all the spatial bins was produced. The activity maps for each individual ESR cell was treated as a vector (list of numbers) and Pearson's correlation between the spatial activity maps of the 2 days was calculated. For the single-day optogenetic inhibition experiment (Fig. 6), the Pearson's correlation was calculated between the spatial activity maps during the light-on trials versus the light-off trials.

Alternative analyses to characterize ESR preservation across sessions. Our ESR correlation analysis showed that ESR activity patterns were highly preserved across sessions, so several analyses were conducted to provide more information about the nature of this ESR preservation. While ESR correlation was treated as a metric for quantifying preservation, we next quantified the percentage of ESR cells that exhibited significant ESR correlation according to a statistically defined criterion. We shuffled the calcium transients of individual cells during the second session 1,000 times according to equation (1) and the description in "Identification of ESR cells". We then calculated the ESR correlation between each cell's session 1 ESR activity pattern and each of the session 2 shuffled ESR activity patterns. Finally, the percentage of cells whose ESR correlation was above the 95th statistical significance level of the shuffled ESR correlations were reported in Supplementary Fig. 4 for all major experiments. All major experiments showed similar results (Supplementary Fig. 4) to those obtained when we used the $r > 0.6$ criterion and compared ESR correlations versus shuffles (Supplementary Fig. 5).

Besides quantifying the preservation of the overall ESR activity patterns by conducting ESR correlation analysis, we quantified the percentage of cells that preserved their lap preference (that is, cells that have maximal activity on lap i and remained maximal on the same lap i during the second session). All major experiments showed similar results (Supplementary Fig. 6) as those obtained using ESR correlation (Supplementary Fig. 5).

Venn diagram display. The Venn diagram display in Supplementary Fig. 2 was constructed using the MathWorks Venn software package (https://mathworks.com/matlabcentral/fileexchange/22282-venn).

Statistics. *Statistical analysis.* Statistical analyses were performed in Matlab (MathWorks). All statistical tests in this study were two-tailed. Single-variable comparisons were made with two-tailed t-tests. Group comparisons were made using analysis of variance (ANOVA) followed by Tukey–Kramer post-hoc analysis. The statistical analyses of calcium events is discussed in detail in the Methods. The numbers of mice for all experiments are reported in the figure legends.

Sample sizes. No statistical methods were used to predetermine sample sizes for single experiments, but the sample sizes were similar to or greater than other studies in the field ($n = 3$–4 animals per experiment, for example, as in refs. [4,16,32]). Most of our experiments included $n \geq 4$ animals unless otherwise indicated in the main text and figures.

Replication and blinding. All experiments reported here were reliably reproduced in individual mice for all calcium imaging and behavioral experiments (Extended Data Fig. 4; Supplementary Figs. 4–6). Data collection and analyses were not performed blind. In all experiments, animals simply ran on the maze while receiving reward. Computer-based analyses ensured unbiased data collection and analyses.

Figure displays. For display purposes, heatmap figures used spatial and temporal smoothing.

Figure 1e and Extended Data Fig. 1b show raw calcium activities organized by spatial location and lap number and used 6.25-cm spatial bins along the 100-cm linear track that were normalized and Gaussian smoothed ($\sigma = 25$ cm). Figures 2d,4e and 6g show raw calcium activities organized by spatial location, and used 6.25-cm spatial bins along the 100-cm linear track that were normalized and Gaussian smoothed ($\sigma = 25$ cm). Figures 1f,2a,4b and 6d, and Extended Data Fig. 1d–f show raw trial-by-trail calcium activities organized by spatial location and lap number and used 6.25-cm spatial bins without smoothing. Figures 2b,3a,4c and 6e, and

Extended Data Figs. 6a, 8d and 10b display two-dimensional spatial plots with $1 \times 1 cm^2$ spatial bins and Gaussian filter $\sigma = 4$ cm.

Figure 7b and Extended Data Fig. 9c show raw calcium activities organized by the time of the calcium activity on the treadmill and the lap number, and used 0.5-s time bins along the 12-s treadmill period that were normalized and Gaussian smoothed ($\sigma = 2$ s). Figure 7d,e shows raw trial-by-trail calcium activities organized by the time of the calcium activity on the treadmill and the lap number, and used 0.5-s time bins without smoothing.

Reporting Summary. Further information on research design is available in the Nature Research Reporting Summary linked to this article.

Data availability

The data, reagents and materials that support the findings of this study are available from the corresponding authors upon request.

Code availability

The code that supports the findings of this study is available from the corresponding authors upon request.

References

50. Mukamel, E. A., Nimmerjahn, A. & Schnitzer, M. J. Automated analysis of cellular signals from large-scale calcium imaging data. *Neuron* **63**, 747–760 (2009).
51. Dombeck, D. A., Harvey, C. D., Tian, L., Looger, L. L. & Tank, D. W. Functional imaging of hippocampal place cells at cellular resolution during virtual navigation. *Nat. Neurosci.* **13**, 1433–1440 (2010).
52. Skaggs, W. E., McNaughton, B. L. & Gothard, K. M. An information-theoretic approach to deciphering the hippocampal code. *Adv. Neural Inf. Process. Syst.* **5**, 1030–1037 (1993).
53. Wills, T. J., Cacucci, F., Burgess, N. & O'Keefe, J. Development of the hippocampal cognitive map in preweanling rats. *Science* **328**, 1573–1576 (2010).

Acknowledgements

We thank M. Wilson, T. Kitamura, J. Z. Young, D. Roy, G. Buzsaki, G. Dragoi, E. Brown, M. Sur, M. Harnett, M. Hasselmo, C. MacDonald, K. Allen, J. Correa, A. Aqrabawi, S. Muralidhar, Q. Ferry, K. Flick, Z. Yang, N. Chen and J. Tao for comments; F. Bushard, C. Twiss, A. Hamalian, C. Ragion, C. Lovett, D. King and Ella Maru Studio for technical assistance; L. Brenner for paper preparation; and the members of Tonegawa Lab for their support. We wish to thank Inscopix, Inc. for scientific collaboration and providing access to the nVoke integrated imaging and optogenetics system. This work was supported by the RIKEN Center for Brain Science, the Howard Hughes Medical Institute, and the JPB Foundation (to S.T.).

Author contributions

C.S. and S.T. designed the study. C.S., W.Y. and S.T. interpreted the data. C.S. and J.M. conducted the surgeries, behavior experiments and computational analyses. C.S., W.Y. and S.T. wrote the paper. All authors discussed and commented on the manuscript.

Competing interests

The authors declare no competing interests.

Additional information

Extended data is available for this paper at https://doi.org/10.1038/s41593-020-0614-x.

Supplementary information is available for this paper at https://doi.org/10.1038/s41593-020-0614-x.

Correspondence and requests for materials should be addressed to C.S. or S.T.

a

Mouse	Laps run	Box visits missed
196	72	0
197	68	0
261	60	0
285	68	0
286	72	0
287	72	0
289	72	0
290	80	0
291	80	0
292	76	0
296	64	0
306	60	0
308	68	0
363	60	0

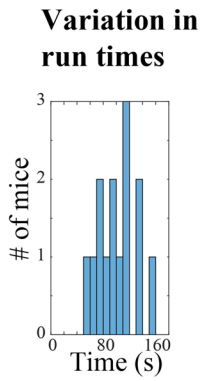

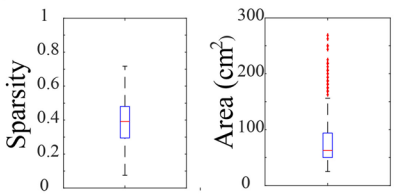

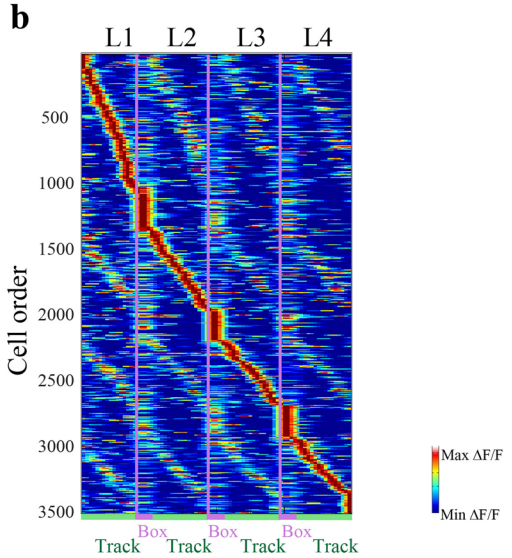

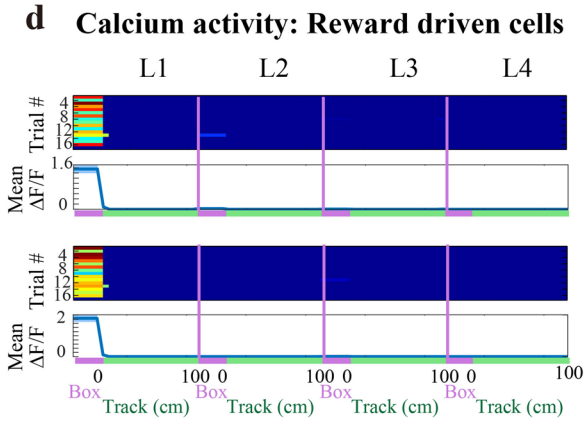

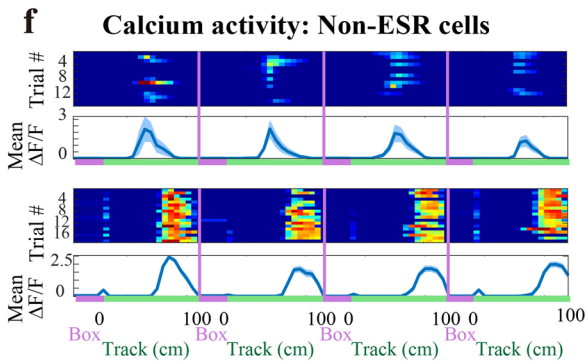

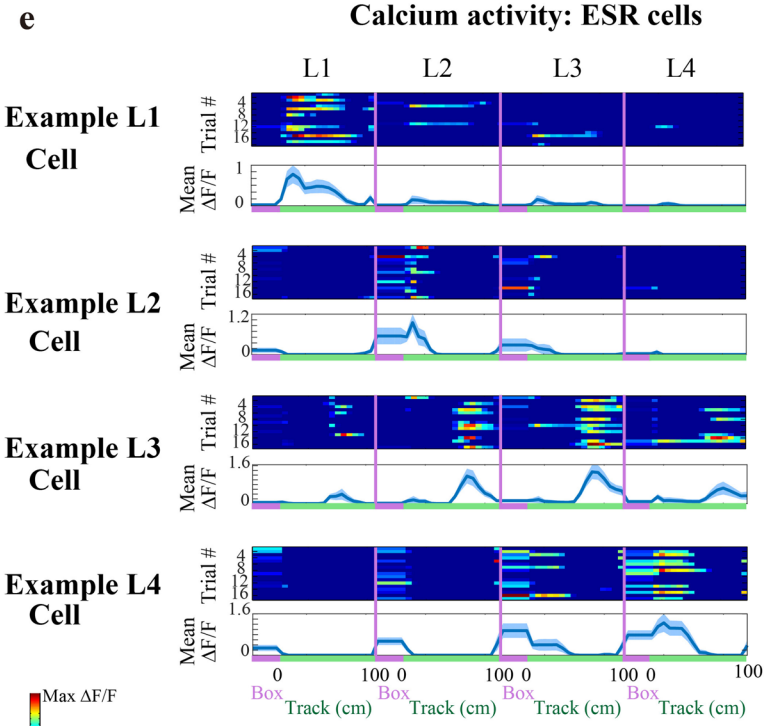

Extended Data Fig. 1 | Spatial and Reward properties of CA1 cells on the maze. a, **Left:** Summary of mice running in a single session of the standard 4-lap-per-trial task. Mice did not miss a visit into the reward box on any run. **Right:** Mean run time among trials (n = 14 animals). **b**, CA1 calcium activity sorted by spatial position and lap number (3506 cells, n = 14 animals). **Red** label indicates reward box spatial bin, and **green** label indicates the 100 cm long maze track. Reward box activity during lap 1 (reward eating period) was excluded. **c**, Characterization of mean spatial properties of CA1 cells active in the lap maze: **Left:** sparsity, and **Right:** spatial field size; n = 14 mice. In total, 72% (2509/3506) of CA1 cells from 14 animals were significant place cells. Box and whisker plots display median, 25th and 75th percentiles (box), and maximum and minimum values (whiskers). **d**—**f**, Spatially binned calcium activity along the track (**d**) 2 example cells that responded to the reward, and (**e**) One example lap 1, 2, 3, and 4 cell each, and (**f**) 2 example place cells that did not have lap modulated activity. **Top** panel: trial-by-trial activity **Bottom** panel: trial-averaged activity with mean ± SEM. The number of trials for each cell is indicated in each figure panel (**d**—**f**). Standard error was cut off at 0 because negative activity does not exist.

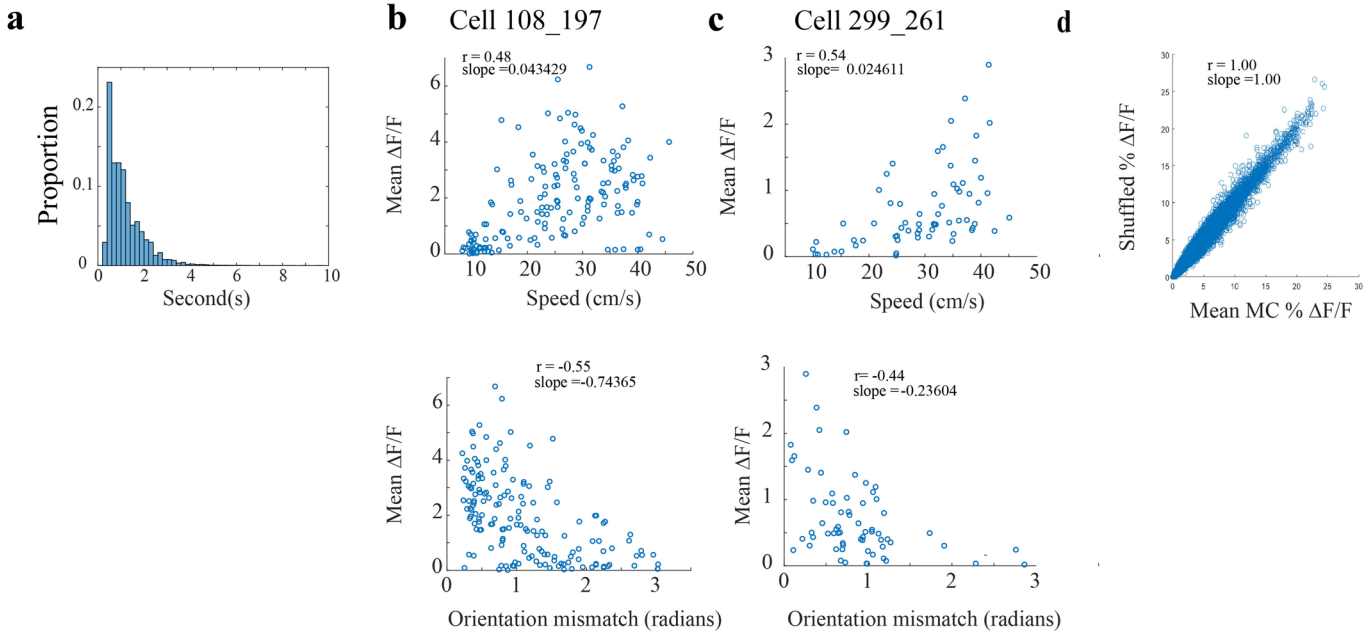

Extended Data Fig. 2 | Model correction for Speed and Head direction modulations of CA1 cell activity. a, The half decay time (the time required for a calcium transient to decay to ½ its maximum height) of 137045 calcium transients across n = 14 animals as they underwent the standard 4-lap task. **b**, – **c**, Two example cells with calcium activity level plotted against mean animal running speed (top subpanels), and head direction tuning (bottom subpanels). *r* denotes Pearson's correlation. (**b**) contains 161 nonzero measurements, and (**c**) contains 54 nonzero measurements of mean calcium activity during the epochs of the experimental session defined in the Methods (subsection "Calcium event filtering"). **d**, Shuffling procedure preserved the mean calcium activity level as prescribed by the linear model (See Methods) (*r* denotes Pearson's correlation. Mean calcium activity measurements taken from 1716479 epochs from all cells recorded during experimental sessions of 14 animals). Epochs are defined in Methods, subsection "Calcium event filtering".

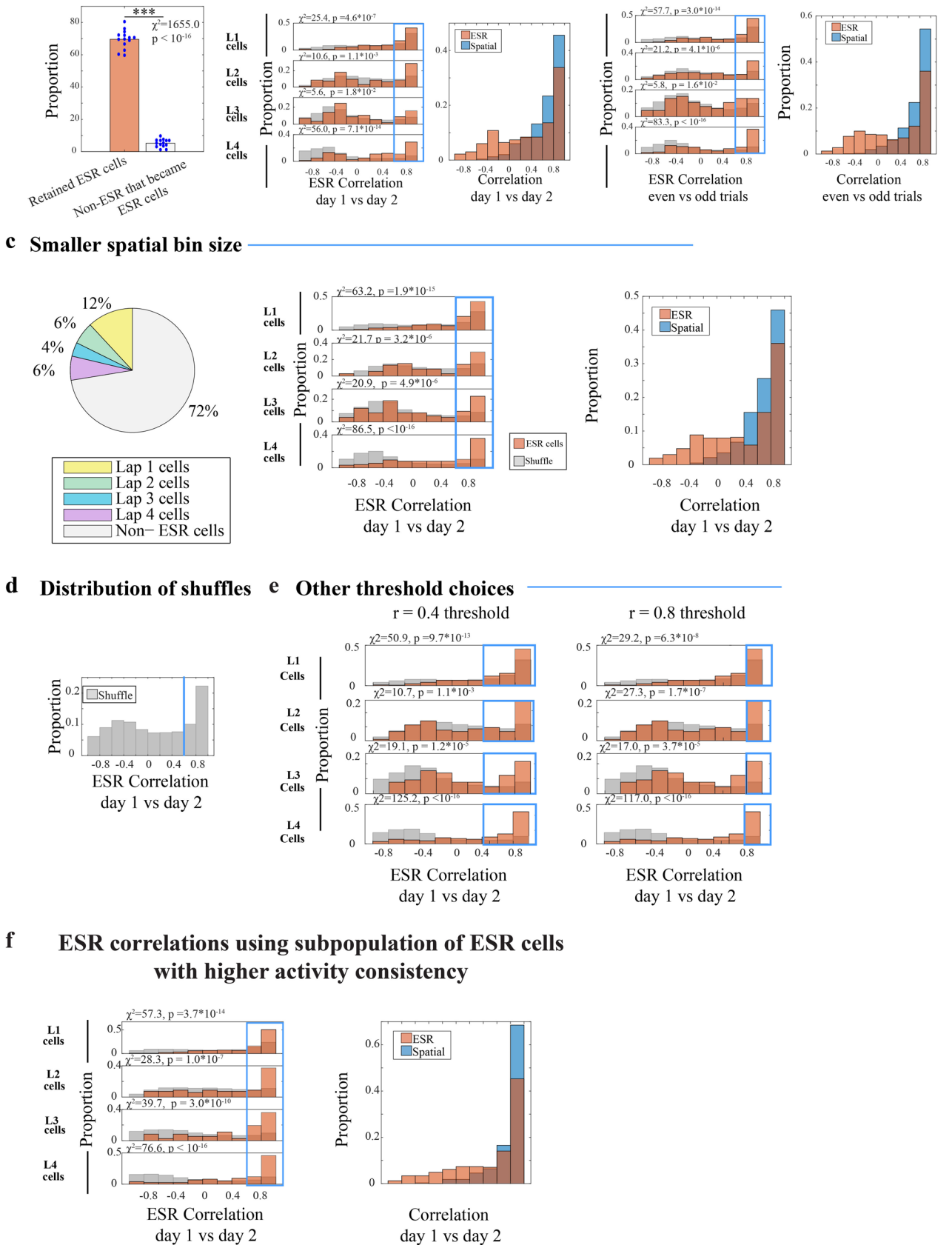

Extended Data Fig. 3 | See next page for caption.

Extended Data Fig. 3 | Robustness of ESR phenomenon to different parameter choices. a, Analysis procedure with a random quarter of all trials (i.e. 4 to 5 trials) during the standard 4-lap experiment removed, for each mouse. **Left:** Percentage of previously statistically significant ESR cells that retained their statistical significance (70% = 726/1055 ESR cells, n = 14 mice) compared to previously non-ESR cells that became significant (5% = 131/2451 cells, same animals). **Middle and Right**: Pearson correlation of ESR activity and spatial activity across days in the standard 4-lap experiment. See Fig. 2(e) for description and methods. (500 cells total). **b**, ESR correlations between even numbered trials vs odd numbered trials of individual cells, as an indicator for the robustness of ESR patterns between trials. See Fig. 2(e) for description and methods. (611 cells total). **c**, Standard analysis procedure conducted on the standard 4-lap experiment (see Methods)—albeit with a smaller spatial bin size (6.25 cm x 5 cm). **Left:** Summary statistics: Percentage of ESR cells in the whole CA1 pyramidal population that were tuned to lap 1, 2, 3, or 4, on a single day in the standard 4-lap experiment (n = 14 animals, 3506 cells). **Center and Right:** Pearson correlation of ESR activity and spatial activity across days in the standard 4-lap experiment (n = 8 animals, 566 cells). **d**, The distribution of ESR correlations when cell identities were shuffled across day 1 vs 2 on the standard 4-lap task (n = 8 mice). **e**, Lap 1, 2, 3, and 4 ESR cells were significantly preserved over days during the standard 4-lap task, even with different thresholds for highly preserved ESR cells. χ^2 and p values are shown in the Figure (622 cells total). **f**, Pearson correlation of ESR activity across days during the standard 4-lap task, calculated using the subpopulation of ESR cells that were active in the main spatial bin during at least 1/2 of all the trials (327 cells total).

Random lap addition experiment

a Random experiment schedule

4 → 4 → 4 → 4 → 4 → 4 → 4 → 5 → 5 → 4 →
4 → 4 → 4 → 5 → 4 → 4 → 4 → 4 → 4 →5

b

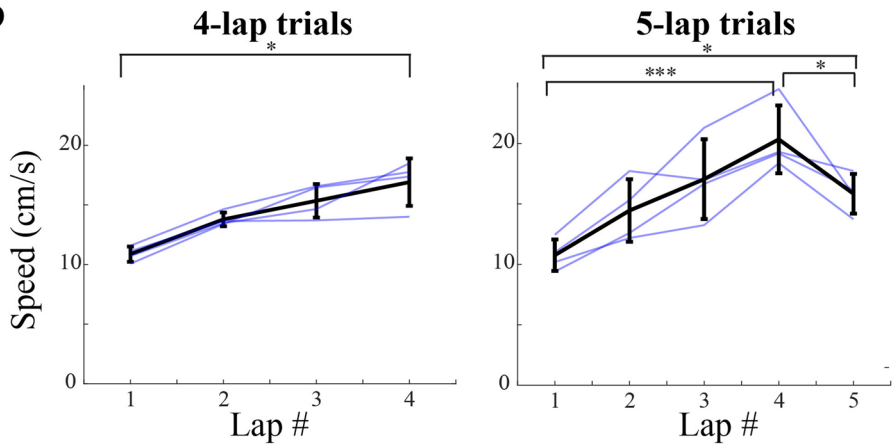

Un-trained vs well-trained experiment

c

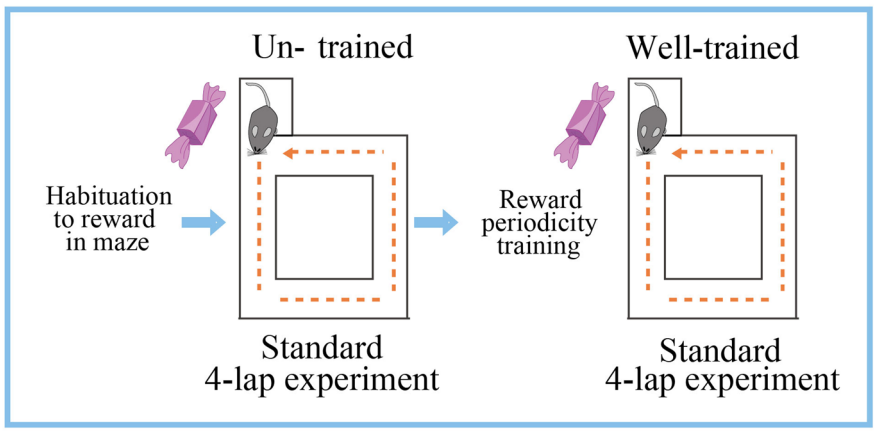

d

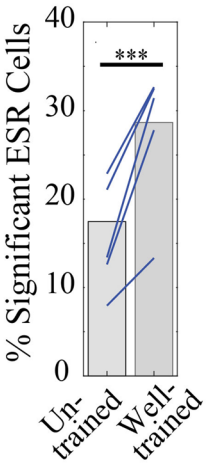

e

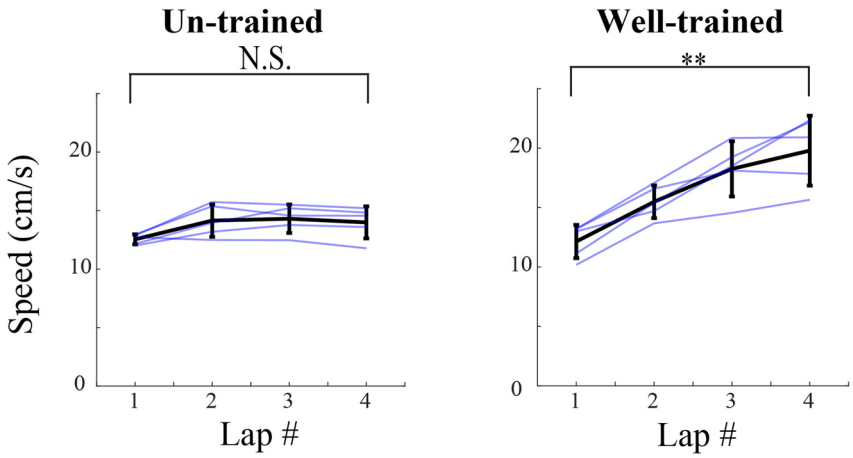

Extended Data Fig. 4 | See next page for caption.

Extended Data Fig. 4 | ESR is learning dependent and indicates recognition of lap number. a, Pseudorandom experiment schedule: 20 trials in total where 4 pseudorandomly chosen trials had an extra (5^{th}) lap before reward delivery. **b**, Mean speed during active periods (defined > 4 cm/s) plotted separately for different lap numbers (**left**) during standard 4-lap trials (lap 4 vs lap 1: Paired T-test: tstat = 5.48, df = 3, $p = 1.2*10^{-2}$), and (**right**) during the unexpected 5-lap trials for the same n = 4 mice (mean ± SD). (One-way ANOVA: $F_{(2,9)} = 22.48$, p = 0.0003. Tukey-Kramer post-hoc analysis for lap 4 vs lap 1: $p = 2.3*10^{-4}$, lap 4 vs lap 5: $p = 2.9*10^{-2}$, lap 1 vs lap 5: $p = 1.5*10^{-2}$). Blue lines indicate speed of individual mice. **c**, Experimental schedule for un-trained vs well-trained animals on the standard 4-lap-per-trial task. **d**, The percentage of significant ESR cells was significantly less during un-trained session (176/1008 cells) comparing with well-trained session in the same mice (335/1168) ($\chi^2 = 37.9$, $p = 7.4*10^{-10}$; **Blue** lines: 5 mice). **e**, Mean active speed (active periods defined > 4 cm/s) plotted separately for different lap numbers (**left**) in un-trained animals (lap 4 vs lap 1: Paired T-test: tstat = 2.29, df = 4, p = 0.084), vs (**right**) the same well-trained animals (n = 5 mice, mean ± SD) (lap 4 vs lap 1: Paired T-test: tstat = 6.42, df = 4, $p = 3.0*10^{-3}$). Blue lines indicate speed of individual mice. * denotes p < 0.05, ** denotes p < 0.01, *** denotes p < 0.001, N.S. not significant.

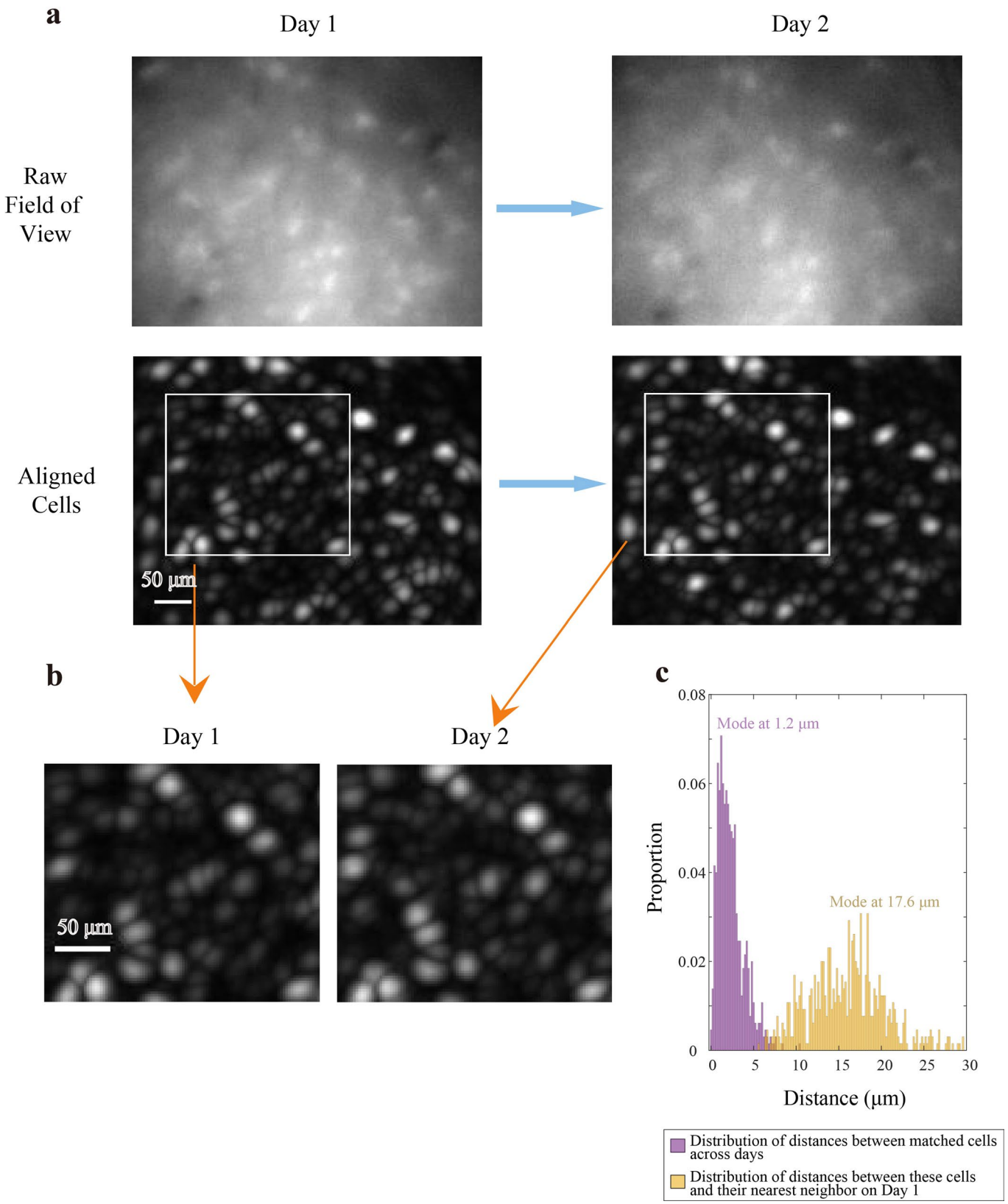

Extended Data Fig. 5 | Method for image registration across days. a, Field of view of raw endoscopic image (**Top**) during day 1 (**Left**) and day 2 (**right**) in one example animal. Corresponding locations of cells (**Bottom**) during the same two sessions, as seen in max projection images after motion correction. Representative of images from n = 4 mice. **b**, Expanded view of aligned cell locations on day 1 and day 2 from (**a**). **c**, **Purple:** Distances between active cells on Day 1 and their putatively matched cells on Day 2 (650 cells, n = 4 animals). **Yellow:** Distances between the same cells and their nearest neighbor within Day 1. Plot is cut off at 30µm.

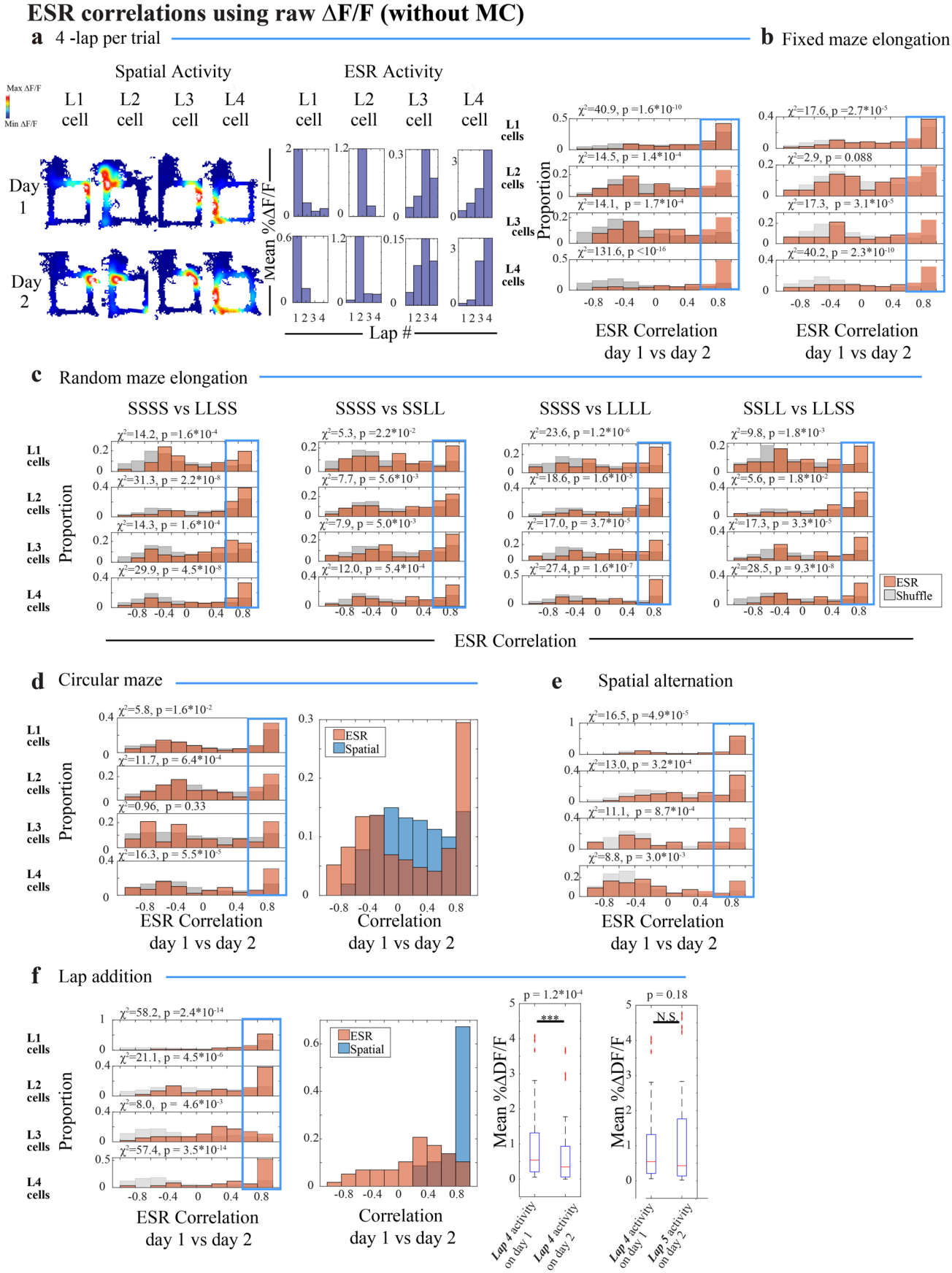

Extended Data Fig. 6 | See next page for caption.

Extended Data Fig. 6 | ESR correlation across sessions as calculated using raw ΔF/F activity without model correction. a, **Left:** The same single example lap 1, 2, 3, and 4 neurons matched across 2 consecutive test days as Fig. 2a–c, measured by raw ΔF/F calcium activity (i.e. without model correction). **Right:** ESR correlation across days, calculated using raw ΔF/F activity. The cells here were the same animals and experimental sessions as Fig. 2 above, plotted separately for lap 1, 2, 3 and 4 cell populations (621 cells total). **b**, – **f**, ESR correlation of individual cells across sessions, calculated using raw ΔF/F activity, for the (**b**) fixed maze elongation experiment from Extended Data Fig. 8 (446 cells), (**c**) random maze elongation experiment from Fig. 3a–f (306 cells), (**d**) circular maze experiment from Fig. 4 (461 cells), (**e**) spatial alternation experiment from Extended Data Fig. 10 (371 cells), (**f**) lap addition experiment from Fig. 5 (378 cells in the first left panel, 58 cells in the second left panel, 41 cells in the two right panels). The cells here were from the same animals and experimental sessions as the corresponding plots in the main Figures, plotted separately for lap 1, 2, 3 and 4 cell populations. (**f**) right two panels: Box and whisker plots display median, 25th and 75th percentiles (box), and maximum and minimum values (whiskers).

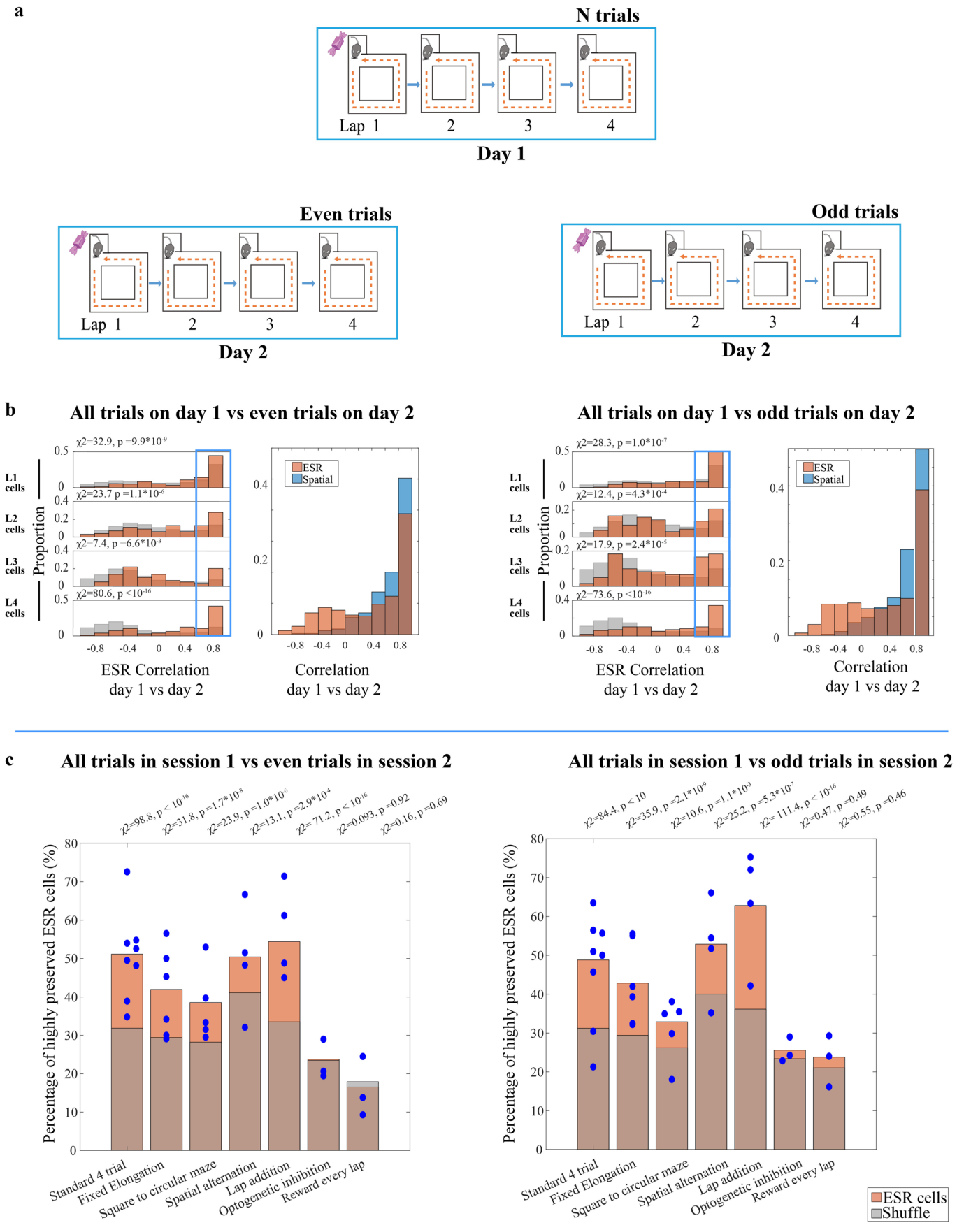

Extended Data Fig. 7 | See next page for caption.

Extended Data Fig. 7 | Robustness of ESR preservation across days. a, ESR correlation analysis of the standard 2-day experiment from Fig. 2(a) above, in which trials during day 2 were separated into even numbered trials, and odd numbered trials. **b**, ESR correlations between (**left**) all trials from day 1 and even numbered trials from day 2, and (**right**) all trials from day 1 and odd numbered trials from day 2, of the standard 2-day 4-lap experiment. See Fig. 2(e) for description and methods. **c**, Proportion of ESR cells that were highly preserved across sessions (**Orange**) (ESR correlation > 0.6) in each experiment, compared to shuffles (**Grey**). ESR correlations were calculated between all trials from session 1 and even numbered trials from session 2 (**left**), and all trials from session 1 and odd numbered trials from session 2 (**right**). Note that in the optogenetic inhibition experiment, session 1 refers to light-Off trials, while session 2 refers to light-On trials. **Blue dots:** shows the proportion of cells for each individual animal, in each experiment. χ^2 and p values are shown in the Figure. (**c**) (**left**): from left to right: 579, 422, 457, 367, 366, 168, 121 total cells respectively. (**c**) (**right**): from left to right: 588, 413, 459, 367, 363, 172, 122 total cells respectively.

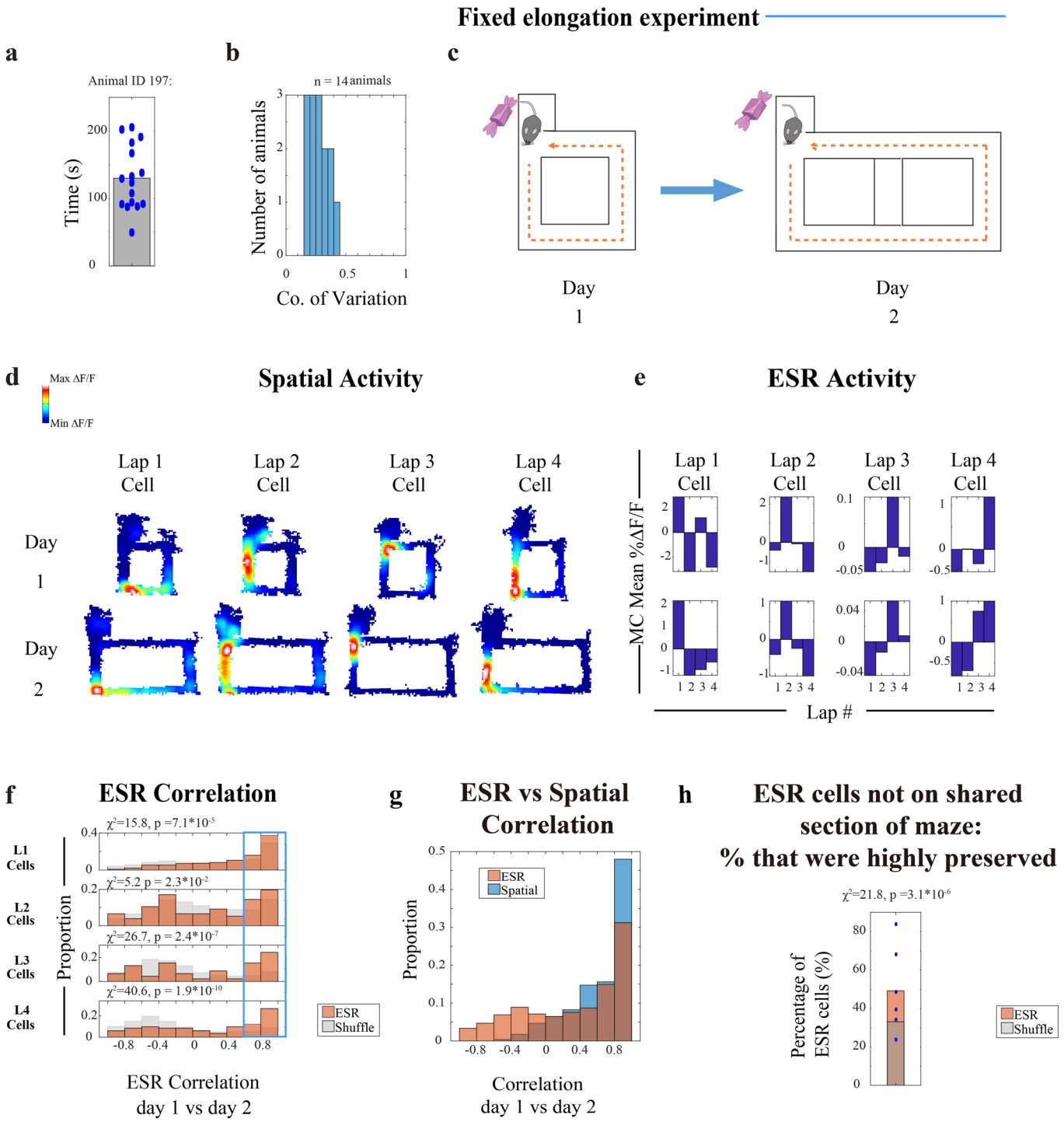

Extended Data Fig. 8 | ESR is unaffected by temporal and spatial variations within events. a, Distribution of running time across trials for animal 197 during 18 trials; **b**, Coefficient of variation $\left(\frac{\sigma}{\mu}\right)$ for running time among trials in n = 14 animals. **c**, Fixed maze elongation experiment: 4-lap-per-trial task on: Day 1: the standard maze and Day 2: the elongated maze. **d**—**e**, Example lap 1, 2, 3, and 4 preferring neurons matched across standard and elongated maze sessions. **f**, ESR correlations across standard and elongated maze sessions (448 cells, n = 6 mice). The proportion of cells with highly preserved ESR patterns across days (Pearson's $r > 0.6$, shown in the **Blue box**) was significantly greater compared to shuffles. **g**, Spatial correlations and ESR correlations across days, during the fixed maze elongation experiment (448 cells). **h**, 185 out of 448 ESR cells had main spatial field not on the shared unstretched half of the maze. Within these 185 cells, 91 cells had highly preserved (Pearson's $r > 0.6$) ESR patterns across days (**Orange bar**) significantly greater compared to shuffles (**Grey bar**). **Blue dots:** shows the proportion of cells for each individual animal. χ^2 and p values are shown in the Figure.

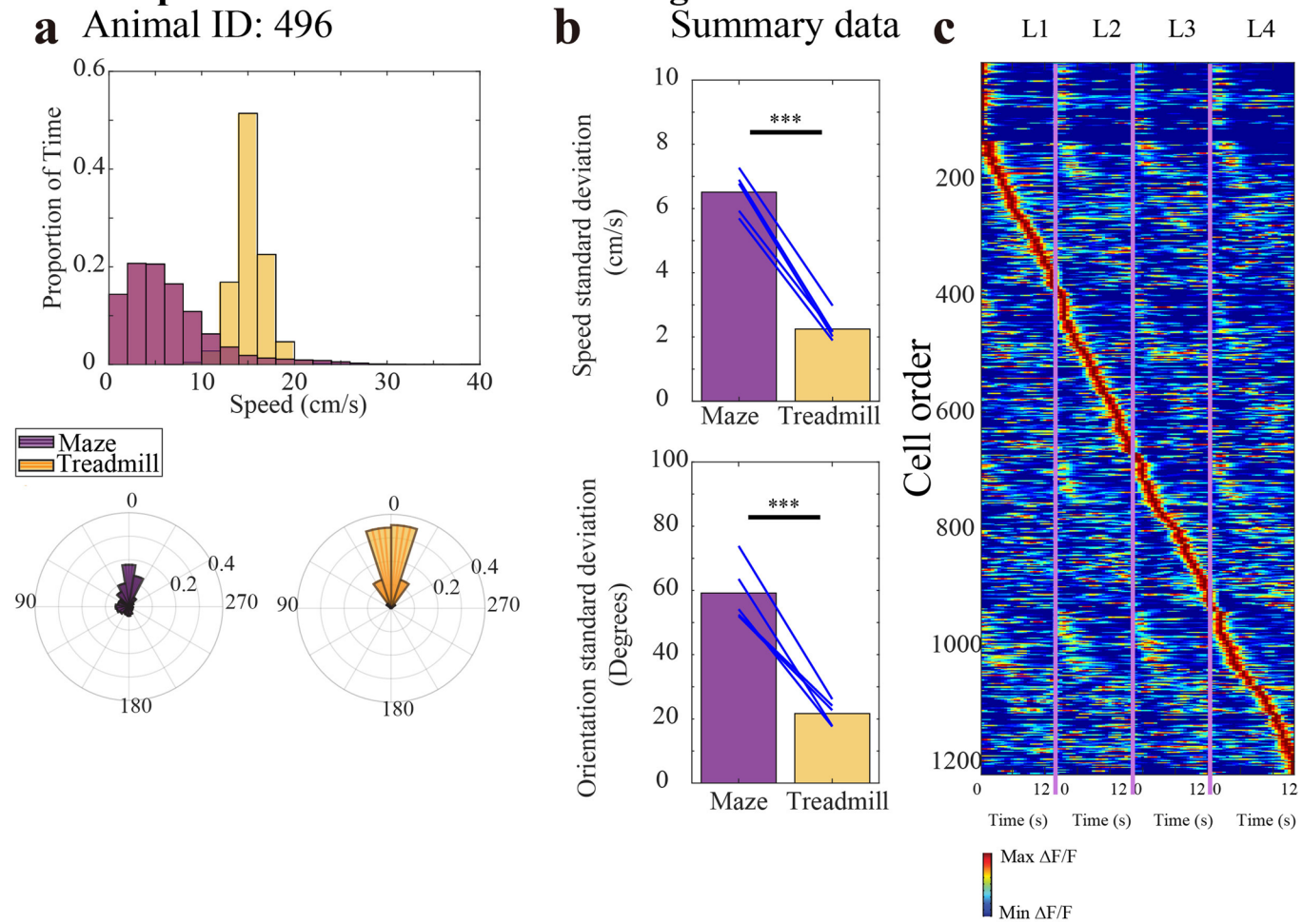

Extended Data Fig. 9 | ESR during the treadmill period. a, Distribution of **top:** animal running speed, and **bottom:** animal head direction during the maze running portion (**purple**) versus the treadmill running portion (**yellow**) of the task, for animal 496 in 20 trials. **b**, Summary data: comparison of standard deviation of **top:** animal running speed (Paired T-test: tstat = 19.65, df = 4, p = 4.0 * 10^{-5}), and **bottom:** animal head direction (Paired T-test: tstat = 9.32, df = 4, p = 7.4 * 10^{-4}) during the maze running portion (**purple**) versus the treadmill running portion (**yellow**) of the task, for 5 animals. **c**, CA1 calcium activity sorted by spatial position and lap number (1222 cells, n = 5 animals).

Spatial alternation experiment

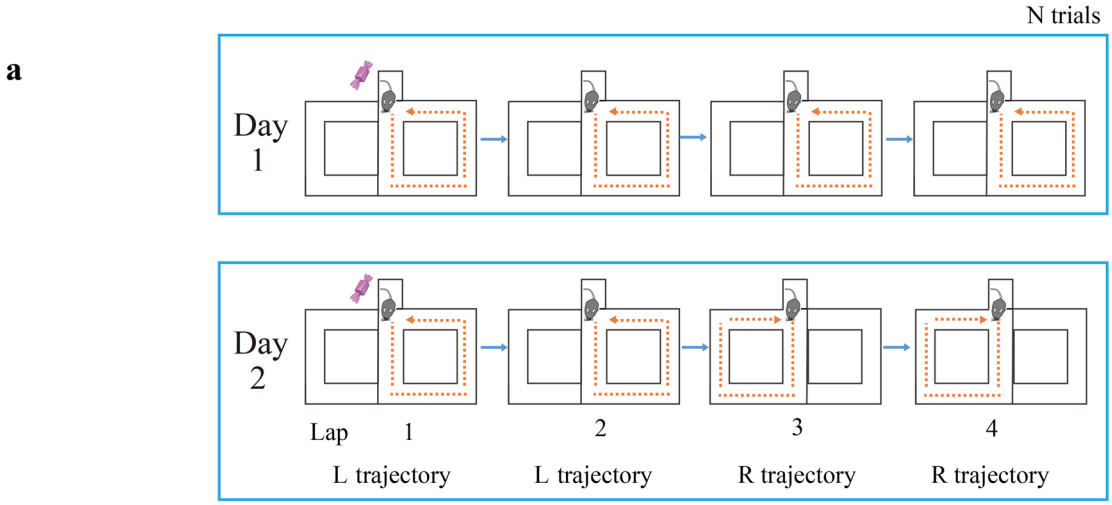

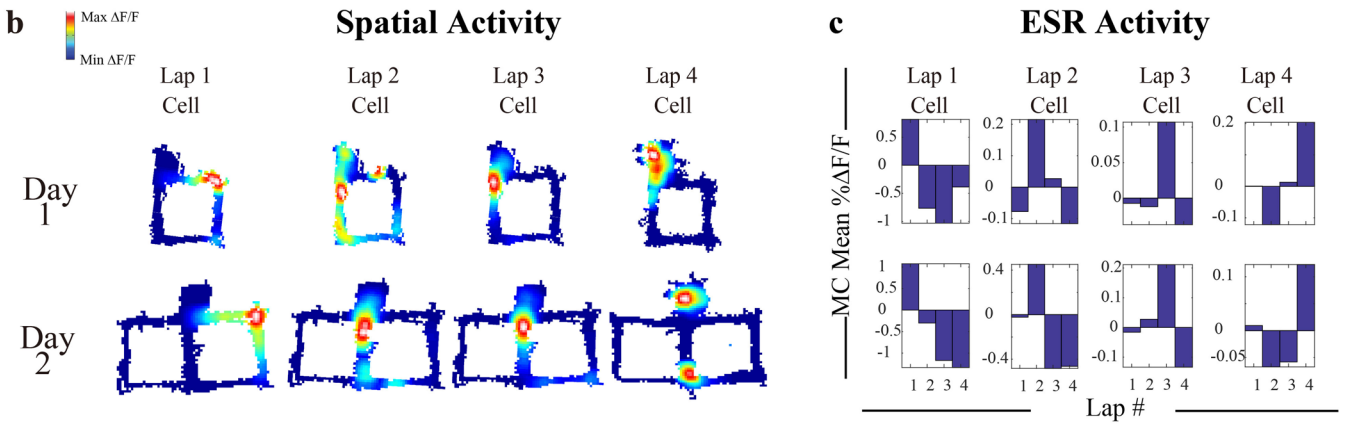

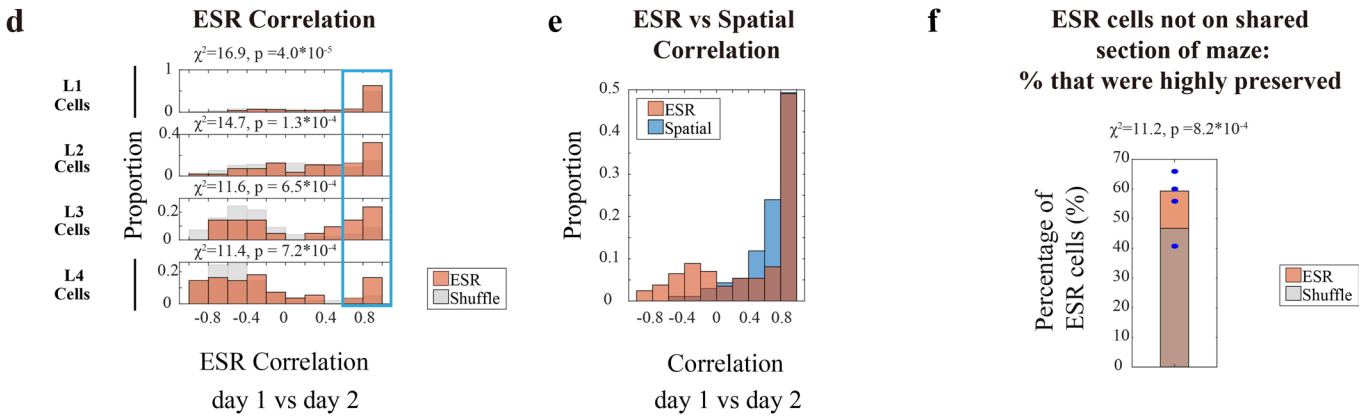

Extended Data Fig. 10 | ESR tracks lap events despite spatial trajectory alternation. a, Alternation experiment: Day 1: standard 4-lap experiment and Day 2: alternating trajectory experiment. **b**—**c**, Example lap 1, 2, 3, and 4 preferring neurons, matched across standard and alternating maze sessions. **d**, ESR correlations across the standard and alternating maze sessions (371 cells, n = 4 mice). The proportion of cells with highly preserved ESR patterns across days (Pearson's $r > 0.6$, shown in the **Blue box**) was significantly greater compared to shuffles. **e**, Spatial correlations and ESR correlations across days, during the alternation experiment (371 cells). **f**, 177 cells out of 371 ESR cells had main spatial field not on the shared unstretched half of the maze. Within these 177 cells, 105 cells had highly preserved (Pearson's $r > 0.6$) ESR patterns across days (**Orange bar**) significantly greater compared to shuffles (**Grey bar**). **Blue dots:** shows the proportion of cells for each individual animal. χ^2 and p values are shown in the Figure.

nature research

Corresponding author(s): Chen Sun
Susumu Tonegawa

Last updated by author(s): Dec 10, 2019

Reporting Summary

Nature Research wishes to improve the reproducibility of the work that we publish. This form provides structure for consistency and transparency in reporting. For further information on Nature Research policies, see Authors & Referees and the Editorial Policy Checklist.

Statistics

For all statistical analyses, confirm that the following items are present in the figure legend, table legend, main text, or Methods section.

n/a	Confirmed	
☐	☒	The exact sample size (*n*) for each experimental group/condition, given as a discrete number and unit of measurement
☐	☒	A statement on whether measurements were taken from distinct samples or whether the same sample was measured repeatedly
☐	☒	The statistical test(s) used AND whether they are one- or two-sided *Only common tests should be described solely by name; describe more complex techniques in the Methods section.*
☐	☒	A description of all covariates tested
☐	☒	A description of any assumptions or corrections, such as tests of normality and adjustment for multiple comparisons
☐	☒	A full description of the statistical parameters including central tendency (e.g. means) or other basic estimates (e.g. regression coefficient) AND variation (e.g. standard deviation) or associated estimates of uncertainty (e.g. confidence intervals)
☐	☒	For null hypothesis testing, the test statistic (e.g. *F*, *t*, *r*) with confidence intervals, effect sizes, degrees of freedom and *P* value noted *Give P values as exact values whenever suitable.*
☒	☐	For Bayesian analysis, information on the choice of priors and Markov chain Monte Carlo settings
☒	☐	For hierarchical and complex designs, identification of the appropriate level for tests and full reporting of outcomes
☐	☒	Estimates of effect sizes (e.g. Cohen's *d*, Pearson's *r*), indicating how they were calculated

Our web collection on statistics for biologists contains articles on many of the points above.

Software and code

Policy information about availability of computer code

Data collection	Inscopix nVista 2.0.4 for calcium imaging video capture Inscopix nVoke 2.1.8 for calcium imaging video capture VirtualDub1.10.4 for behavior video processing Zeiss ZEN (black edition) software for histology acquisition
Data analysis	MATLAB 2017a for calcium imaging data analysis and analysis of behavior ImageJ 1.52a for calcium imaging data analysis and analysis of behavior Inscopix Mosaic 1.2.0 for calcium imaging data analysis

For manuscripts utilizing custom algorithms or software that are central to the research but not yet described in published literature, software must be made available to editors/reviewers. We strongly encourage code deposition in a community repository (e.g. GitHub). See the Nature Research guidelines for submitting code & software for further information.

Data

Policy information about availability of data

All manuscripts must include a data availability statement. This statement should provide the following information, where applicable:

- Accession codes, unique identifiers, or web links for publicly available datasets
- A list of figures that have associated raw data
- A description of any restrictions on data availability

The data that support the findings of this study are available from the corresponding authors upon request.

Field-specific reporting

Please select the one below that is the best fit for your research. If you are not sure, read the appropriate sections before making your selection.

☒ Life sciences ☐ Behavioural & social sciences ☐ Ecological, evolutionary & environmental sciences

For a reference copy of the document with all sections, see nature.com/documents/nr-reporting-summary-flat.pdf

Life sciences study design

All studies must disclose on these points even when the disclosure is negative.

Sample size	No statistical methods were used to pre-determine sample size but the sample sizes matched or exceeding those reported in previous studies in the literature (n = 3 animals). Most of our experiments included n >= 4 group sizes unless otherwise indicated in the main text and figures.
Data exclusions	Pre-established criteria: Experimental sessions were excluded if the animal missed visiting the box more than once during the session (as Described in the Methods section "Apparatus description and experimental conditions").
Replication	All experiments were consistent across individual animals. Furthermore, most experiments were "variations" of a basic novel behavioral task, and they showed similar results.
Randomization	Animals were randomly assigned to experiments.
Blinding	Data collection and analysis were not performed blind. In all experiments, animals simply ran on the maze while receiving reward. Computer-based analyses ensured unbiased data analysis.

Reporting for specific materials, systems and methods

We require information from authors about some types of materials, experimental systems and methods used in many studies. Here, indicate whether each material, system or method listed is relevant to your study. If you are not sure if a list item applies to your research, read the appropriate section before selecting a response.

Materials & experimental systems

n/a	Involved in the study
☒	☐ Antibodies
☒	☐ Eukaryotic cell lines
☒	☐ Palaeontology
☐	☒ Animals and other organisms
☒	☐ Human research participants
☒	☐ Clinical data

Methods

n/a	Involved in the study
☒	☐ ChIP-seq
☒	☐ Flow cytometry
☒	☐ MRI-based neuroimaging

Animals and other organisms

Policy information about studies involving animals; ARRIVE guidelines recommended for reporting animal research

Laboratory animals	Species: Mouse (Mus musculus) Strain: Wfs1-Cre mice and pOxr1-Cre mice Sex: Male Age: 2-4 months
Wild animals	The study did not involve wild animals
Field-collected samples	The study did not involve field-collected samples
Ethics oversight	All procedures were all performed in accordance with Massachusetts Institute of Technology (MIT)'s Committee on Animal Care guidelines and NIH guidelines.

Note that full information on the approval of the study protocol must also be provided in the manuscript.